SANDIA REPORT
SAND2001-0101
Unlimited Release
Printed January 2001

Thin-Skin Deployable Mirrors for Remote Sensing Systems

Tammy D. Henson, Joseph C. Wehlburg, James M. Redmond, John A. Main, and Jeffrey W. Martin

Prepared by
Sandia National Laboratories
Albuquerque, New Mexico 87185 and Livermore, California 94550

Sandia is a multiprogram laboratory operated by Sandia Corporation, a Lockheed Martin Company, for the United States Department of Energy under Contract DE-AC04-94AL85000.

Sandia National Laboratories

Issued by Sandia National Laboratories, operated for the United States Department of Energy by Sandia Corporation.

Available to DOE and DOE contractors from
U.S. Department of Energy
Office of Scientific and Technical Information
P.O. Box 62
Oak Ridge, TN 37831

Telephone: (865)576-8401
Facsimile: (865)576-5728
E-Mail: reports@adonis.osti.gov
Online ordering: http://www.doe.gov/bridge

Available to the public from
U.S. Department of Commerce
National Technical Information Service
5285 Port Royal Rd
Springfield, VA 22161

Telephone: (800)553-6847
Facsimile: (703)605-6900
E-Mail: orders@ntis.fedworld.gov
Online order: http://www.ntis.gov/ordering.htm

SAND 2001-0101
Unlimited Release
Printed January 2001

Thin-Skin Deployable Mirrors for Remote Sensing Systems

Tammy D. Henson and Joseph C. Wehlburg
Remote Sensing and Exploitation Department

James M. Redmond
Structural Dynamics Development and Smart Systems Department

Sandia National Laboratories
P.O. Box 5800
Albuquerque, NM 87185-0980

John A. Main and Jeffrey W. Martin
Department of Mechanical Engineering
University of Kentucky
Lexington, KY 40506-0108

Abstract

Meeting the long term needs of the DOE nonproliferation mission as well as future space exploration initiatives requires the development of large aperture space based optical systems to achieve dramatic improvements in resolution and sensitivity. While many researchers are considering on-orbit assembly of rigid optical mirror segments to circumvent geometric limitations imposed by launch vehicles, their volumetric and weight constraints limit the aperture diameter to less than ~10 meters. Therefore, ultra large apertures will likely only be obtained using deployable thin-skin mirror technology. Ultra large deployable thin-skin mirrors may offer orders of magnitude improvement in resolution and sensitivity over what is achievable today, yet many technological barriers must be overcome to make this approach a viable alternative for future system designs. Of primary concern is the development of control methodologies for achieving and maintaining optical tolerances from a highly flexible surface. This report summarizes an initial research effort into the development of piezoelectric thin-skin mirrors. A thin-skin piezoelectric bimorph mirror will bend in response to an applied electric field and can therefore be deformed into desirable shapes using a scanning electron gun. Recent progress is described in the key areas of experimental testbed development, mirror figure sensing methods, electron gun excitation, and shape control algorithm development. Results show that although this field of research is in its infancy, many of the technological barriers to realization of a deployable mirror are surmountable. Continued research in this field is warranted on the basis of its potential for dramatically improving the resolution and sensitivity of future space based optical systems.

ACKNOWLEDGMENTS

The authors would like to thank John Hunter, Pat Barney, and Bruce Hansche of Sandia National Laboratories for their contributions to this research program. Also, the assistance of Lenore McMackin and her colleagues at the Air Force Research Lab is greatly appreciated. We would also like to thank Steve Wojtkiewicz and Karen Jefferson of Sandia who provided thoughtful technical reviews of this report.

CONTENTS

FIGURES

TABLES

EXECUTIVE SUMMARY

Large aperture optics are critical for improving sensitivity and ground resolution of future space based telescope systems, such as those needed to monitor global proliferation of weapons of mass destruction (WMD). However, the cost and configuration of existing launch vehicles currently limit aperture size. Development of deployable mirrors is one approach being considered to satisfy the conflicting requirements for low cost and large optical apertures. At present the leading concepts overcome geometric limitations through assembly of rigid mirror segments on orbit. Apertures up to approximately 10 meters could potentially be achieved in a single launch, but larger mirrors are not obtainable without first addressing the fundamental weight constraint imposed on space systems. Ultra large apertures will therefore likely be achieved only through deployable thin-skin mirror technology.

Ultra large deployable thin-skin mirrors may offer orders of magnitude improvement in resolution and sensitivity over what is achievable today due to their sheer size, yet many technological barriers must be overcome to make this approach a viable alternative for future system designs. Of primary concern is the development of control methodologies for achieving and maintaining mirror shapes at optical tolerances from a highly flexible surface.

One approach to this problem is to integrate the deployability and shape control directly into the mirror material by making it out of a “smart material” such as a piezoelectric bimorph. A bimorph mirror consisting of piezoelectric material layers with opposite poling will bend in response to an applied electric field and can therefore be deformed into desirable shapes. Controlling specific regions on the mirror can be accommodated by applying segmented electrodes to both surfaces of the bimorph. However, the number of discrete electrodes needed to attain optical quality (tens of thousands per square meter) from a flexible film is prohibitive since the spatial resolution on the shape control is equal to the electrode size.

The deployable thin film optics team has been investigating the use of electron guns to remotely adjust the shape of piezoelectric thin film mirrors to overcome this fundamental limitation of precision shape controlled optics. Since the electric field in the material changes only at the point of electron gun incidence, high resolution distributed shape modification is achieved by scanning the gun across the piezoelectric film according to a feedback control algorithm. Thus the need for huge numbers of individual discrete actuators that would normally be required to attain high-resolution surfaces from flexible films is mitigated. Secondary electron yield characteristics can be manipulated to permit the addition or removal of surface charge at the point of electron beam incidence, enabling positive and negative curvature corrections. Furthermore, the electron gun is ideally suited for space and the power requirements to operate the gun are achievable from a space platform. Consequently, this approach shows great promise for meeting NASA’s long term areal density goals of < 1 Kg/m^2.

The goal of this two-year laboratory directed research and development (LDRD) project was to develop fundamental technology toward the realization of deployable electron-gun-controlled piezoelectric thin-skin mirrors that can be compactly stowed for launch,

deployed on orbit, and shaped to optical tolerances. In this report, progress is described in the key areas of experimental testbed development, mirror figure sensing methods, electron gun excitation, and shape control algorithm development.

A complete experimental testbed was developed at Sandia to provide a means to assess the interaction between the thin-skin bimorph mirror shape and the electron gun excitation. The testbed development was critical not only in determining achievable optical quality, but in calibrating the positional changes in the shape of the bimorph mirror as a function of electron gun parameters such as energy and electrode potential. The testbed includes an 18 inch diameter vacuum chamber, electron gun, optical sensors, bimorph mirrors, and associated electronics. This experimental facility will be the focus of continuing research progressing toward distributed shape control of thin-skin mirrors.

The interaction of the electron gun and the piezoelectric film was studied through a series of controlled experiments. Secondary electron yield characteristics of a Polyvinylidene Fluoride (PVDF) bimorph film were explored through manipulation of the electrode potential and the material behavior was quantified. In addition, a single input single output closed-loop control experiment was conducted using electron gun excitation and a tip displacement measurement. Open-loop shape correction algorithms were developed using computer simulation. Using experimentally derived models, these algorithms solve the direct inverse problem to determine distributed excitations needed to correct surface profile errors. Verification experiments will be conducted in FY01 with the goal of developing a model-independent autonomous closed-loop controller.

Achieving an optical quality surface from a deployable mirror hinges on the ability to accurately assess mirror figure on orbit. The inherent flexibility of these mirrors limits their deployment accuracy to within 1mm of the desired shape. This accuracy is sufficient for long wavelength antenna applications, but is 4 to 5 orders of magnitude larger than the accuracy needed for optical telescopes. Following deployment, the shape of the thin film mirror must therefore be corrected to within the allowed tolerances in order to achieve the needed image quality. Consequently, the required optical sensor must have a dynamic range of 5 orders of magnitude and be capable of resolving the surface profile to 25 nm accuracy.

To satisfy the immediate need for continued laboratory based development of the electron gun while working toward stringent specifications of future flight hardware, both coarse (~50 μm) and fine (~25 nm) measurement systems have been implemented. Coarse surface profile measurements were obtained with the Multi-beam Optical Stress Sensor (MOSS) system and a Keyence LK-2500 series charge coupled device (CCD) laser displacement sensor. Fine surface profile measurements were obtained with electronic speckle pattern interferometry (ESPI), and a multi-wavelength heterodyne interferometer. Application of these techniques proved the capability of the electron gun to make both fine (~100 nm) and coarse (~1mm) surface profile corrections. Realizing the needed dynamic range in a single measurement system will require further progress in the area of multi-wavelength heterodyne interferometry. This technique was briefly examined in this program, but shows great promise as a full field measurement technique with adjustable resolution.

This work has captured the interest of the remote sensing community. Results show that although this field of research is in its infancy, many of the technological barriers to realization of a deployable mirror are surmountable. The potential for dramatically improving the resolution and sensitivity of future space based optical systems warrants continued research in this field. Remaining technical issues to be considered include mirror packaging and deployment, space environment effects on candidate mirror materials, high fidelity shape sensing methods, and robust distributed curvature compensation algorithms. These critical technical issues will continue to be studied in order to bring this technology to maturity.

NOMENCLATURE

AFRL	Air Force Research Lab
ATA	Applied Technology Associates
CCD	charge coupled device
DC	direct current
DoD	Department of Defense
ESPI	electronic speckle pattern interferometry
GPIB	general purpose interface bus
LDRD	laboratory directed research and development
LFTC	Laser Time Flash Control
MOSS	Multi-beam Optical Stress Sensor
NASA	National Aeronautics and Space Administration
NGST	Next Generation Space Telescope
PID	Proportional Integrator Derivative
PVDF	Polyvinylidene Fluoride
PZT	Lead Zirconate Titanate (piezoelectric ceramic)
WMD	weapons of mass destruction
a_i , b_i , c_i , and d_i	spline coefficients
b	bimorph width
d_{31}	piezoelectric voltage constant along length (meter/volt)
d_{32}	piezoelectric voltage constant along length (meter/volt)
e_{31}	piezoelectric field constant along length (coulomb/meter^2)
$E_3(x)$	axially distributed electric field
E_I	Energy at which the ascending electron yield curve equals one
E_{II}	Energy at which the descending electron yield curve equals one
E_{pmax}	Energy of the maximum electron yield
F_t	top surface coupling function
F_b	bottom surface coupling function
G_t	top surface coupling function
G_b	bottom surface coupling function
I	area moment of inertia
$I(x,y)$	ESPI image
K	intensity scaling constant for ESPI system
$M(x)$	internal moment
n	number of measured slopes
s_i	distance between the MOSS sample and the detector
t	bimorph thickness
t_g	thickness of the glue layer
t_p	thickness of piezoelectric ply sheet
$u(x)$	beam sample transverse deflection
$u'(x_i)$	beam sample local surface slope
$u''(x)$	beam sample corrective curvature
$u_d''(x)$	desired beam curvature
$u_m''(x)$	measured beam curvature

$V(x)$	voltage applied across the PZT bimorph ply
$V_c(x)$	distributed corrective excitation profile for PZT bimorph beam
V_t	excitation on top surface of PZT plate
V_b	excitation on bottom surface of PZT plate
x_i	location on MOSS sample where ray reflection occurs
Y	Young's modulus
$Z_R(x,y)$	reference object position for ESPI system
$Z_D(x,y)$	displaced object position for ESPI system
α	incident angle of MOSS ray
$d(x,y)_{\mathrm{mod}(2p)}$	wrapped phase image for the ESPI system.
$d(x,y)$	continuous phase image for the ESPI system.
Δ_i	distance between the nominal and actual spot locations on the MOSS camera
ε_{11}^{top}	axial strain on the top surface
ε_{11}^{bot}	axial strain on the bottom surface
γ_x	curvature along the x direction
γ_y	curvature along the y direction
λ	wavelength of light
λ_1	wavelength one
λ_2	wavelength two
λ_s	synthetic wavelength
θ_i	local slope of deformed MOSS sample

This page intentionally left blank.

Thin-Skin Deployable Mirrors for Remote Sensing Systems

1. INTRODUCTION

The ultimate limitation in resolution and sensitivity for space-based telescope systems is the size of the optical collecting aperture. Large aperture optics are critical for improving sensitivity and ground resolution of future space based telescope systems, such as those needed to monitor global proliferation of weapons of mass destruction (WMD). In particular, there is a need for low cost surveillance satellites that can be quickly launched and positioned in orbit to monitor rapidly evolving events almost anywhere on the globe. However, the desire for low cost and flexibility is in opposition with the requirement for large apertures, which usually imply large, expensive launch vehicles to accommodate the size of the primary mirror. Development of a deployable mirror is one approach being considered to satisfy these conflicting requirements. Folded up and carried on a small booster, the mirror would open to its full diameter in orbit. Unfortunately, the inherent flexibility of such a device makes it difficult to achieve optical quality surfaces, and this approach has therefore not yet been proven feasible.

Fueled by both National Aeronautics and Space Administration (NASA) and Department of Defense (DoD) interests, much of the on-going research in deployable optics is focused on precision assembly of rigid mirror segments (Greschik, 1996). Deployable mirror concepts such as those proposed for the Next Generation Space Telescope (NGST) rely on essentially rigid segments that are stacked or folded for launch. Once on orbit, the full mirror is assembled and various measures are employed to ensure precision alignment and to enable some degree of wavefront correction. These approaches could provide a significant improvement in system performance compared to a single mirror design such as the Hubble Space Telescope, but their volumetric and weight constraints limit their economy to applications requiring less than ~10 meter aperture diameter. Furthermore, it is unlikely that these techniques are capable of meeting the long term areal density goals (~1 Kg/m^2) established by the NASA Gossamer telescope study group (Moore, 1999).

Meeting the needs of the post NGST missions hinges on advances in the field of thin-skin optics that can be compactly launched and deployed to operating diameters of up to 50 meters. Deployable thin-skin mirrors offer orders of magnitude improvements in resolution and sensitivity as compared to today's most sensitive tools, yet many technological barriers must be overcome to make this approach a viable alternative for future system designs. Inflatable optics offer very large diameters with readily available deployment techniques (Rapp, 1996), but the inflated mirror suffers from the 'w' error that indicates a deviation from a desirable paraboloidal shape (Marker, et al., 1998). In addition they suffer from the added complication of diffraction from passing light rays through a gaseous medium. Continuing research in this area is focusing on additional shape correction and rigidization techniques as well as signal processing methods for improved image quality.

Thin-skin mirrors are made from very thin sheets of a flexible material. For any thin-skin optic a primary concern is the development of control methodologies for achieving and maintaining optical tolerances from such a highly flexible surface. Structural shape control, which has been a topic of research among the Adaptive Structures community for two decades, offers many potential benefits to the growing field of large space-based optics. For example, some researchers have implemented smart material actuators to generate mirror distortions at discrete locations that correct for atmospheric disturbances (Hardy et al., 1997, Merkle, 1992). Regional shape corrections are enabled by bonding active materials to the substrate, but still this technique provides shape control at only the actuator locations (Sato et al., 1980 and Steinhaus et al., 1979). This limitation has led investigators to consider integrating the deployability and shape control directly into the mirror material by making it out of a "smart material" such as a piezoelectric bimorph. A bimorph mirror consists of piezoelectric material layers with opposite poling that bend in response to an applied electric field and can therefore be deformed into desirable shapes (Morgan Matroc, 1993). Controlling specific regions on the mirror can be accommodated by segmenting the electrodes (Susini et al., 1995, Forbes et al., 1989), but the number of discrete electrodes needed to attain optical quality (tens of thousands per square meter) from a deployable mirror is prohibitive.

To overcome this fundamental limitation of precision shape controlled optics, the deployable thin film optics team is investigating the use of electron guns to remotely adjust the shape of piezoelectric thin film mirrors (Hubbard, 1992). This revolutionary approach to shape control may enable performance never before achieved with space-based optical systems. The electron gun provides for a noncontact high-resolution approach to remotely changing the shape of the deployed mirror, mitigating the need for myriads of individual discrete actuators required to get high-resolution surfaces from flexible films. Secondary electron yield characteristics can be manipulated to permit the addition or removal of surface charge at the point of electron beam incidence (Main, et al, 1998). Since current flows to or away from the surface only at the point of incidence as shown in Figure 1-1, high resolution distributed shape modification is achieved by scanning the gun across the piezoelectric film according to a feedback control algorithm. Furthermore, the electron gun operation is ideally suited for the space environment and the power requirements to operate the gun are achievable from a space platform. Consequently, this approach shows great promise for meeting NASA's long term areal density goals of < 1 Kg/m^2.

The goal of this two-year laboratory directed research and development (LDRD) project was to develop fundamental technology toward the realization of deployable electron-gun-controlled piezoelectric thin-skin mirrors that can be compactly stowed for launch, deployed on orbit, and shaped to optical tolerances as shown in Figure 1-2. The main thrusts of this program have been experimental testbed development, mirror figure sensing methods, electron gun excitation experiments, and shape control algorithm development. Each of these interdependent efforts are summarized in this report.

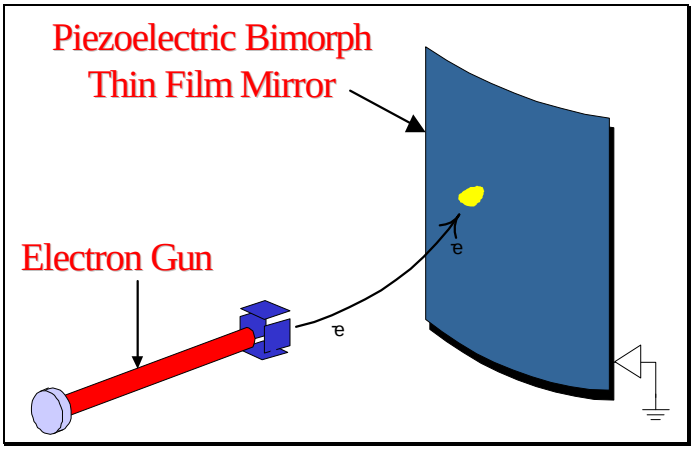

Figure 1-1. Electron-gun-controlled Piezoelectric thin-skin mirror concept**.**

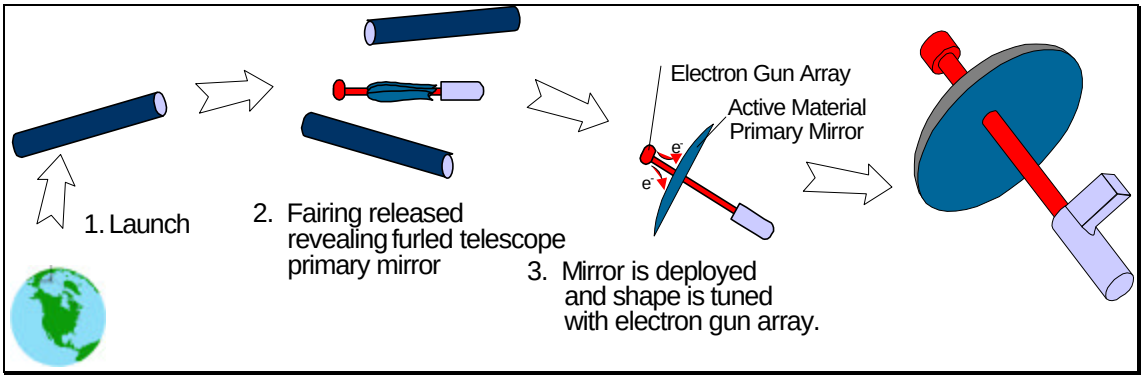

Figure 1-2. Deployment sequence for a large aperture electron-gun-controlled piezoelectric thin-skin bimorph mirror**.**

This page intentionally left blank.

2. BACKGROUND

Piezoelectric materials are a unique classification of "smart materials" which respond directly to an applied electric field across their thickness. The internal dipoles of the material change their alignment in the presence of the applied field and this induces internal micro scale strains that are seen as shape changes on a macro scale. Thus, piezoelectric materials contract or expand in response to an applied electric field, depending on the direction of the material poling relative to the field. A bimorph (Morgan Matroc, 1993) consists of two layers of piezoelectric material with opposite polling. Such a device exhibits a change in curvature in the presence of an electric field. An electron gun can therefore be used to remotely adjust the profile of a bimorph.

2.1 Bimorph Mechanics

In order to develop a functional bimorph mirror a clear understanding of bimorph mechanics must be established. Many related works have been published on this subject (for example Crawley et al., 1986, Hagood et al., 1995, Main et al., 1993, Martin, 1998, Tzou, 1989, Wang et al., 1991). The polarization of the two layers in the specimen should be opposite one another in order to induce bending during piezoelectric control as shown in Figure 2-1.

In controlling a bimorph mirror it is useful to understand the relationship between the applied electric field, E_3 and the transverse deflection, $u(x)$. It can be shown that the transverse deflection for a serially wired bimorph as a function of the position x is given by (Martin, 1998)

$$u(x) = \frac{3}{2}\left[\frac{e_{31}E_3}{Y}\left(\frac{t^2 - t_g^2}{t^3}\right)\right]x^2. \qquad \text{(eq 2.1)}$$

where e_{31} is the piezoelectric constant, E_3 is the applied electric field, Y is Young's modulus, t is the thickness of the bimorph mirror, and t_g is the thickness of the epoxy layer**.** Equation 2.1 shows the significant role that the glue layer plays in stiffening the bimorph beam. In the case of films, the glue layer contributes significantly to the bimorph thickness and should, therefore, be included for accurate performance predictions. For ceramics, the glue layer is often insignificant, and can be neglected to yield

$$u(x) = \frac{3}{2}\left(\frac{e_{31}E_3}{Yt}\right)x^2. \qquad \text{(eq 2.2)}$$

2.2 Electron Gun Excitation

Electron guns are used to supply continuous charge to large distributed areas in a number of systems, the most common of which is the television. In electron gun control of

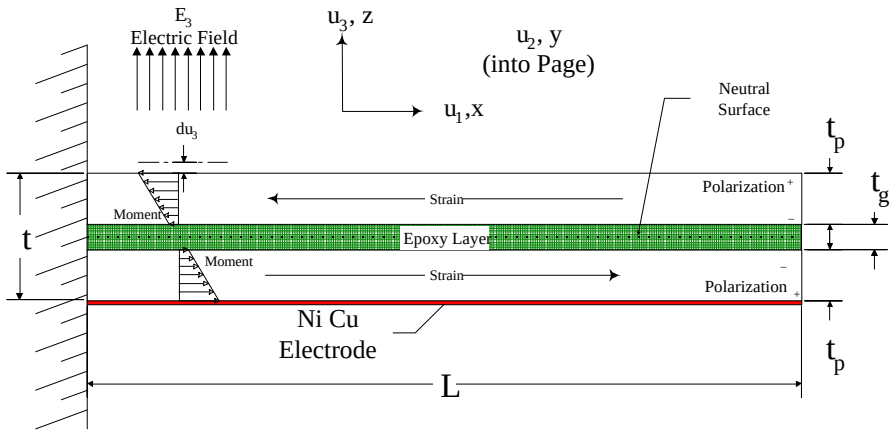

Figure 2-1. PVDF bimorph bending diagram.

piezoelectric materials the electron gun serves precisely the same purpose. Unlike the television, where the electrons incident on the front surface of the tube are absorbed by a phosphor layer and quickly re-radiated as visible light, electron gun control of piezoelectric materials takes advantage of the fact that piezoelectric materials are dielectrics, accumulating a surface charge when exposed to an electron flux (for example NASA 1994). The charge accumulation remains relatively static upon removal of the electron beam, diminishing very slowly as the charge leaks through the surface.

The change in surface charge that results from the collision of the electron with the surface of a piezoelectric material is not as simple as the addition of one electron-sized negative charge. An electron is decelerated when it impacts a surface, giving up its kinetic energy to the material. A number of things can happen to that energy, including raising the energy levels of the electrons already present on the surface to the point that they are ejected as secondary electrons (Goldstein 1977). The number of secondary electrons emitted from a surface due to the impact of a single electron is a function of the energy of the incident electron and the electrode potential.

Figure 2-2 shows a plot of the secondary electron yield for a typical material as a function of the incident electron energy (Whetten 1981, Koshida 1983). The presence of the secondary electron effect gives electron gun control the ability to apply net positive and net negative charges to the surface of the piezoelectric material. The critical points on the curve in Figure 2-2 with regard to electron gun control of piezoelectric materials is the energy level where the ascending electron yield curve equals one (E_I and E_{II}) and the energy of the maximum electron yield (E_{pmax}). Applying electrons with energy between E_I and E_{II} is equivalent to applying a net positive charge to the surface facing the electron gun. Charge equilibrium is reached when enough positive charge accumulates on the surface to bring the impact energy of the incoming electrons up to E_{II}. The approach used in this investigation requires only a single energy electron gun with electron emission energy between E_I and E_{II}. The beam current is used simply to establish current flow between the bare piezoelectric material and the electron gun. The current direction is established by selecting the potential on the other side of the bimorph structure. The incoming electrons “sense” this potential and react by either speeding up (increase in energy level) or decelerating (decrease in energy

level). The accelerated electrons tend to "bounce" off the surface and remove other electrons with them in the process, while the decelerated electrons tend to "stick" to the surface. It is this mechanism that is used to either cause large secondary emissions (conventional current toward the piezoelectric material) or little to no secondary emissions (conventional current away from the piezomaterial). This is illustrated in Figure 2-3. In this method the control potential is applied by varying the potential of the distributed electrode on the other surface. Since the current loop is closed only at the location where the electron beam is incident, only that location experiences piezoelectric strain in response to the change in electrode potential.

Conventional piezo elements have electrodes on both external faces. The electric field across the thickness of the material is adjusted through the application of voltages on these electrodes. The net applied voltage across the material induces piezoelectric strains. These strains result in changes in the material, such as dimensional or stiffness changes. In electron gun control, electron loss from the surface results in a larger electric field, E_3. This induces piezoelectric strains that are seen in the production of bimorph curvature. This enables direct curvature adjustments of the bimorph. Since the electron gun is only used to close the current loop, point specific charge adjustments and therefore curvature changes can be achieved. This ability to deliver minute charge packets to discreet areas causes increased control flexibility and improved spatial resolution over previous electrode pattern-type charge application procedures.

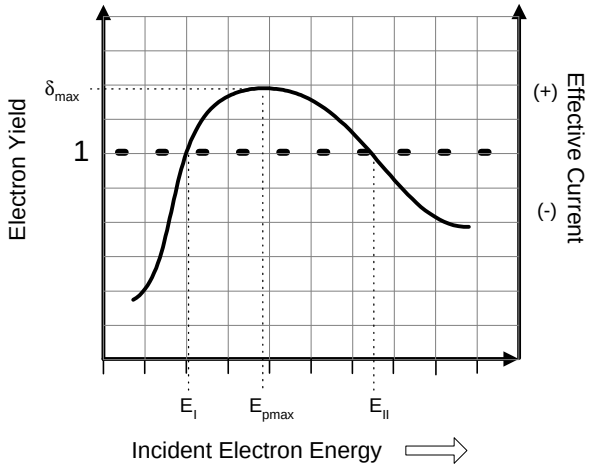

Figure 2-2. Secondary electron yield for a dielectric**.**

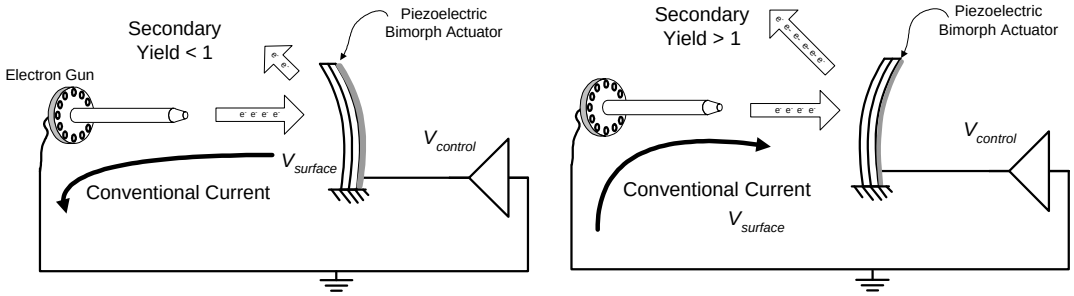

Figure 2-3. Illustrations of the conventional current direction as a function of secondary electron yield in electron gun control**.**

2.3 Implementation Issues

In examining possible implementation issues of a large ultra-lightweight deployable thin-skin piezoelectric mirror in a space-based remote sensing system, we reviewed several items. We briefly investigated what piezoelectric mirror materials would be appropriate for space use. We reviewed the literature to study possible folding methods for the deployable mirror. We also looked at whether or not there were any inherent problems with operating an electron gun on a satellite system.

The most attractive mirror material for space appears to be piezoelectric polyimides because of their robustness in the face of the hostile climate. However, they are expensive and not yet readily available. Polyvinylidene fluoride (PVDF) was judged to be a suitable alternative for our experimental development since it possesses properties similar to the polyimides and is readily available. Further research into potential space qualified piezoelectric polyimide mirror materials and the effect of the space environment (temperature dependence and radiation effects) on their piezoelectric properties and its susceptibility to space particle damage is still needed.

The first mirror structure considered in this study was a one-piece shell which can be folded or rolled into a compact package before launch and then deployed upon reaching orbit by releasing stored elastic energy. Similar concepts for shell antennas were presented by Rogers et al. (1993). This deployable antenna was furled by rolling the entire composite antenna dome into a cylindrical bundle. While this approach does reduce reflector size, it does so in only one dimension. The current effort is focussing on the shell reflector deployment concepts by Greschik (1996). These designs considered one-piece shell reflectors that deploy from a state where significant elastic energy is stored in the structure due to folding. Deployment occurs when the folding forces are removed and the strain energy is released. Stowing of a large reflector in a small, compact package is accomplished in this case by placing discontinuities (cuts) in the mirror surface to permit the mirror to fold in like a flower. Further investigation into possible folding methods and achievable packed to unpacked mirror diameter is still needed.

Using the electron gun and power supply in space should not be a problem. In the past, Sandia National Laboratories and others have flown high voltage power supplies (up to 5KV) as bias supplies for detectors. These power supplies have been as small as 1”x3.5”x7” so this will not cause a problem. The expected power demand for the electron gun would be ~10W to produce the needed electron beam. Though this is high for a single component it is not a showstopper. The ability of the electron gun to function in space is not in question because the systems are normally operated in a vacuum and some can be baked out to 350^{o} C. So it appears there are no inherent problems with operating an electron gun in space. The electron gun may cause a direct current (DC) bias offset in unshielded electronic components when it is operating. Therefore, the potential for electrical interference and its impact on other satellite components should be investigated.

3. SANDIA EXPERIMENTAL TESTBED

A complete experimental testbed has been developed at Sandia to provide a means to assess the interaction between the thin-skin bimorph mirror shape and the electron gun excitation. The testbed development was critical not only in determining achievable optical quality, but in calibrating the positional changes in the shape of the bimorph mirror as a function of electron gun parameters such as energy and electrode potential. The testbed includes a vacuum system, electron gun, optical sensors, bimorph mirrors, and associated electronics. Figure 3-1 shows the testbed system with the Electronic Speckle Pattern Interferometer (ESPI) measuring the shape changes induced in the bimorph mirror by electron gun excitation. Optical measurements of the electron gun controlled bimorph mirrors were used to calibrate the mirrors and as input to a feedback control system.

3.1 Vacuum System

One of the constraints of electron gun control of distributed structures, is the need for a vacuum. The high temperature of the electron gun element would cause it to malfunction if it were exposed to atmospheric conditions. Most electron guns have an operating pressure lower than 1.0×10^{-6} Torr. It is this rarified atmosphere that prevents oxidation of the gun filament. This equipment, which can be difficult to maintain, is the basis for electron gun control research.

3.1.1 Chamber

A stainless steel .039 m^3 chamber was used. This chamber is rated to hold a vacuum of 1.0×10^{-12} Torr. All fittings were seated using ConFlat flanges with solid copper gaskets to maintain the highest possible vacuum. Access to the experiment between pump downs was facilitated using a 45.7 cm viewport door from Kurt J. Lesker Co. This avoided the tedious removal of the 28 bolts holding down the 45.7 cm flange each time the chamber was accessed.

3.1.2 Pumping

Evacuation of the chamber is done in two stages. The initial pump down, or roughing stage, was done using a Varian model DV-2 dry diaphragm pump. This model maintains a pressure of 1.0×10^{-3} Torr on the outlet port of the Turbo molecular pump. The Turbo pump, 2^{nd} stage, is a Varian V60 turbo molecular pump. This model is designed to maintain pressures in an ideal system as low as 1.0×10^{-12} Torr.

Much of the experimental work was done on thin-skin mirrors. Vibrations due to the turbo pump and the roughing pump cause low amplitude high frequency vibrations that skew high-resolution data. A 300 L/sec third stage ion pump, which was manufactured by Varian, was added to the system. This pump is capable of maintaining pressures of up to 1.0×10^{-14} Torr by bonding air molecules to internal cathodes, thereby lowering pressure through non-mechanical means, which generate no vibration. When the system reaches operating

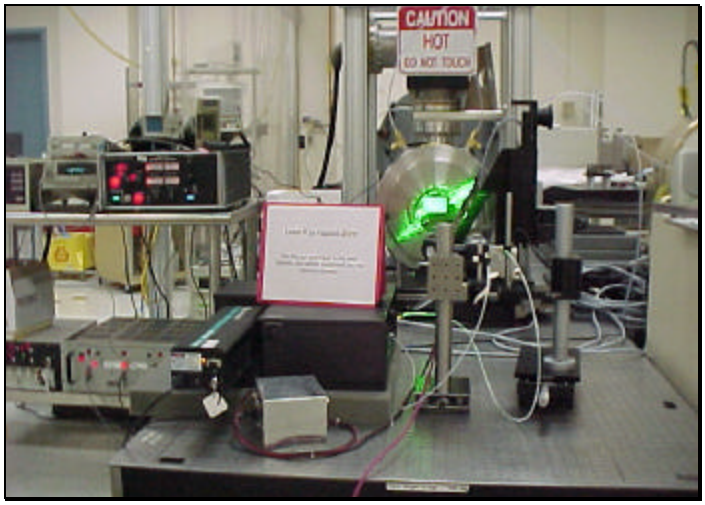

Figure 3-1. Sandia experimental test bed setup.

pressures, the chamber and ion pump were then isolated, and both the turbo and roughing pump were removed.

3.1.3 Pressure Measurement

In electron gun control, pressure must remain below the working pressure of the electron gun. An Ion gauge is used to accurately measure the pressure within the vacuum chamber. Ion gauges have a working measurement from $1.0x10^{-3}$ Torr to ultra-high vacuum pressures. At higher pressures, the element of the ion gauge burns out.

Thermocouples are widely used to measure from atmospheric pressure (760 Torr) down to $1.0x10^{-3}$ Torr. A vacuum gauge controller, like the Varian SenTorr, is used to constantly monitor the pressure readings. This controller automatically turns on/off the ion gauge at the correct set-point pressure, which prevents damage to the equipment.

3.2 Electron Gun

The model EFG-7 electron gun, serial # EFG-7-4690 was manufactured by Kimball Physics Inc. of Wilton, New Hampshire. This model is capable of placing a focused electron beam spot as small as 1mm in diameter on any point on the research specimens with a variable electron energy range of 400-1500 eV. This particular electron gun has an operating pressure of 10^{-5} to 10^{-11} Torr. The electron gun power supply, also manufactured by Kimball Physics Inc., is a model EGPS-7, serial #EGPS-7H-474. This model provides variable energy, focus, source current, and grid voltages. The beam deflection uses a four pole electrostatic system that can also be adjusted by ±5° maximum for a 1500 eV electron beam in both the X and Y direction.

The EFG-7 electron gun from Kimball Physics needs 6 signals to allow complete computer control of all the electron gun's operating parameters: energy (beam voltage), current (beam current), grid, focus, x deflection, and y deflection (Kimball Physics Inc., 1997). The control system developed was used to calibrate electron beam location as a

function of energy and deflection voltages for the x-axis and the y-axis. The results are shown in Figures 3-2 and 3-3. The displacement of the electron beam is linear for the different energies, so the electron gun beam position based on x and y deflection voltages for the different energies are easy to calculate. This data was integrated into the control system so the user can select locations instead of deflection voltages.

The EFG-7 model electron gun can achieve a spot size of approximately 1 mm at 800 eV energy. The settings to achieve a small spot size for the EFG-7 electron gun are shown in Table 3-1.

3.3 Control System

A 600 megahertz PC, LabView 5.1 programming language, a National Instruments PCI-6713 A/O board, a PCI-MIO-16E-1 A/I board, and an AT-GPIB board were used to develop an automated control system. This system was created to remotely control and take data from the electron gun power supply, KEPCO BOP-1000M power amplifier, Newport precision x-y-z staging system, Keithley 480 picoamp meter, and two Hewlett Packard 3325A function generators. Currently programs exist to create grid patterns with the electron gun, draw functions with the electron gun, and create a fixed spot of variable size. Using the controls that we have constructed, large area or point changes can be made to a bimorph. Further programs have been developed to perform the needed experiments for bimorph voltage versus energy calibrations without user intervention.

Table 3-1. EFG-7 electron gun settings for small spot size.

eV	Current	Grid	Focus	Comments
1500	9	86	6.502	Small
1400	9	79	6.098	Small
1300	9	74	5.764	Medium Small
1200	9	66	5.184	Small
1100	9	60	4.895	Small
1000	9	55	4.408	Small
900	9	47	3.961	Small
800	9	42	3.483	Small
700	9	38	3.001	Small
600	9	29	2.684	Small
500	9	25	2.183	Small
400	9	4	1.880	Large

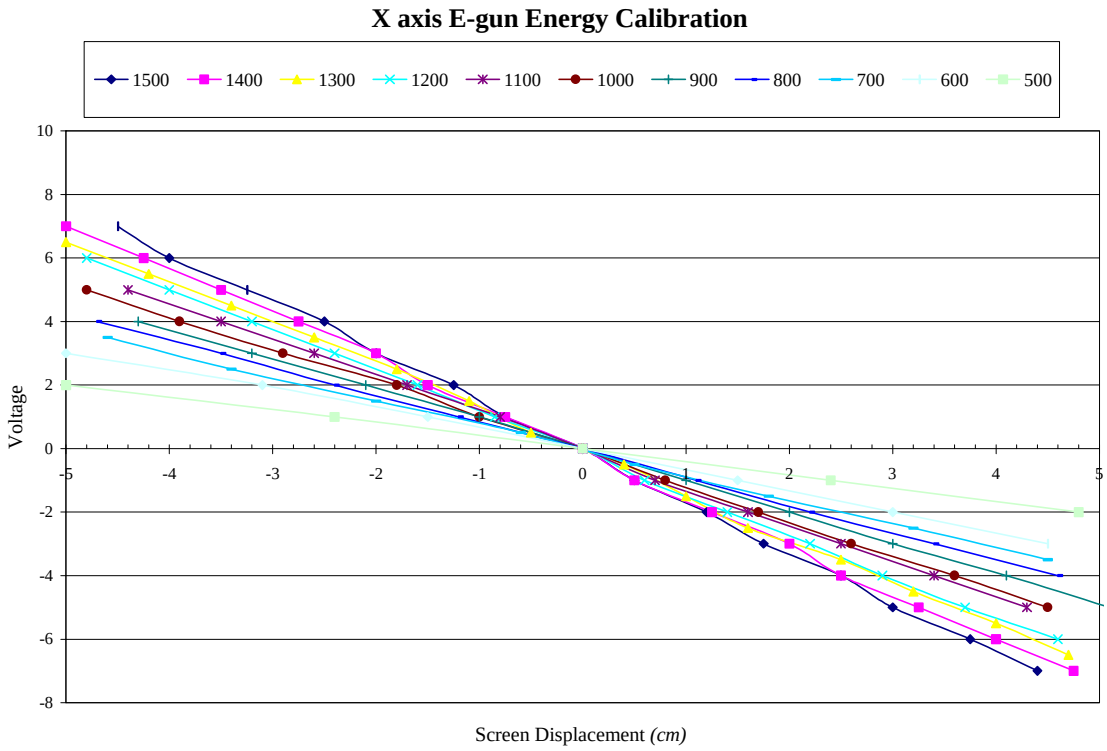

Figure 3-2. X-axis calibration data for the EFG-7**.**

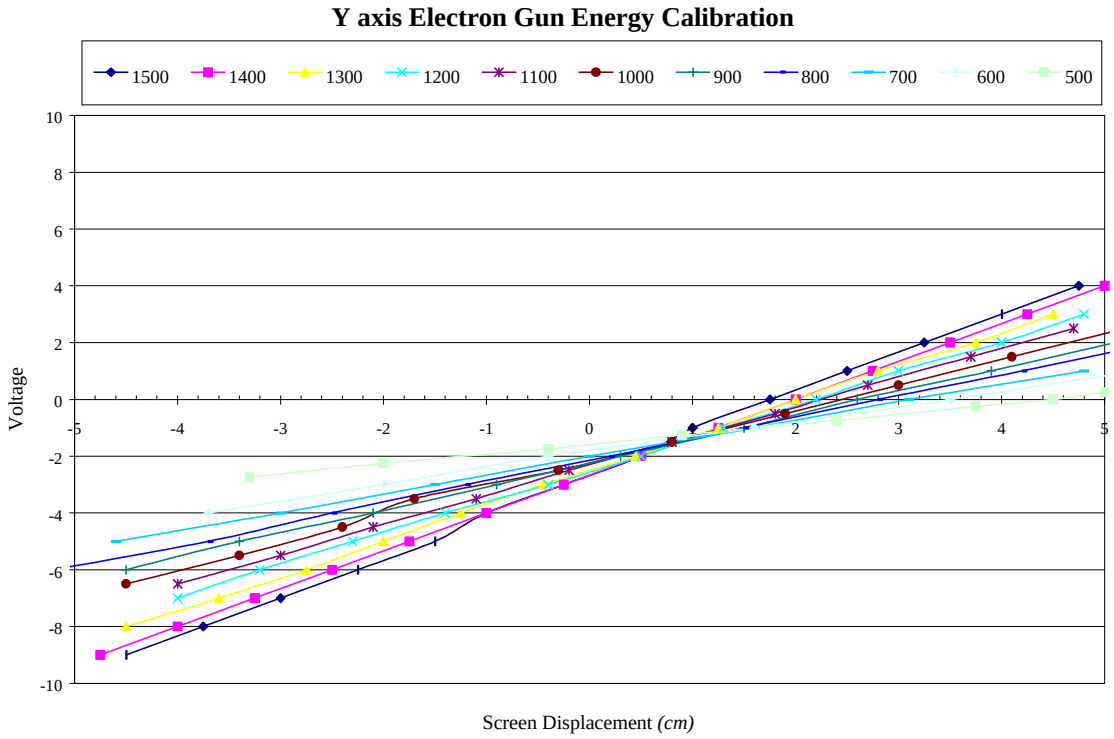

Figure 3-3. Y-axis calibration data for the EFG-7**.**

4. MIRROR FIGURE SENSING METHODS

Achieving an optical quality surface from a deployable mirror hinges on the ability to accurately assess mirror figure on orbit. The inherent flexibility of these mirrors limits their deployment accuracy to within 1mm of the desired shape (Rapp, 1996). This accuracy is sufficient for long wavelength antenna applications, but is 4 to 5 orders of magnitude larger than the accuracy needed for optical telescopes. Following deployment, the shape of the membrane mirror must therefore be corrected to within the allowed tolerances in order to achieve the needed image quality. Consequently, the required optical sensor must have a dynamic range of 5 orders of magnitude and be capable of resolving the surface profile to 25 nm accuracy.

To satisfy the immediate need for continued laboratory based development of the electron gun while working toward stringent specifications of future flight hardware, both coarse (~50 μm) and fine (~25 nm) measurement systems have been implemented. Coarse surface profile measurements were obtained with the Multi-beam Optical Stress Sensor (MOSS) system developed by Sandia Org. 1112 and a Keyence LK-2500 series charge coupled device (CCD) laser displacement sensor. Fine surface profile measurements were obtained with electronic speckle pattern interferometry (ESPI) developed at Sandia Org. 9122, and a multi-wavelength heterodyne interferometer developed by researchers at the Air Force Research Lab (AFRL) and at Applied Technology Associates (ATA).

4.1 MOSS System

A technique for obtaining coarse resolution profiles of deformable mirrors was developed through modification of the Multi-beam Optical Stress Sensing (MOSS) system (Floro et al., 1995 and Robinson, 1998). Originally developed to monitor stresses in semiconductor films during deposition processes, this technique can provide surface profiles by modifying the data reduction procedure. Using discrete slope measurements inferred from the MOSS data, a shape estimation algorithm has been developed based on the cubic spline curve fitting technique. This approach was successfully implemented on a lead zirconate titanate piezoelectric ceramic (PZT) wafer deformed under varying excitation levels.

4.1.1 MOSS System Overview

The Multi-beam Optical Stress Sensor (MOSS) system was developed by researchers in the Nanostructure and Semiconductor Physics Department at Sandia for the purpose of monitoring stresses in thin films during their growth process. A schematic diagram of the MOSS system is shown in Figure 4-1. After some spatial filtering, a Helium-Neon laser beam is passed through an etalon. This optical device has a partially transmissive reflective coating on its outer surfaces, allowing it to capture the light and reflect it internally. At each reflection, a portion of the beam leaks through the outer surface, resulting in an array of parallel beams that reflect off the sample. While only the one-dimensional implementation is

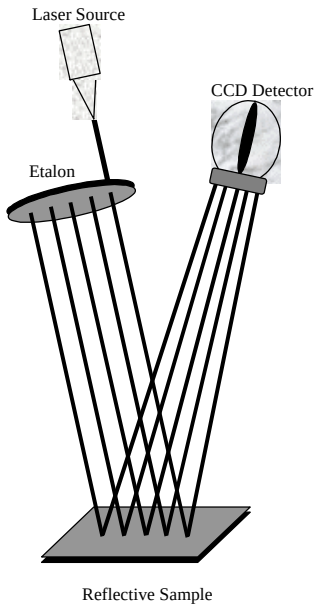

Figure 4-1. Diagram of the Multi-beam Optical Stress Sensor (MOSS) system.

presented here for simplicity, insertion of a second etalon askew to the first yields a two-dimensional array of beams, enabling surface profiling.

The reflected light rays are captured at the CCD camera positioned approximately 0.66 m above the sample surface. The essence of the MOSS system is computing the centroids of the spots on the camera pixel array and comparing the mean differential spacing of the spots to that of an optical flat. This measurement provides an estimate of the sample radius of curvature, which is used to determine film stress. The sensitivity of the system is dependent on the geometric parameters of the hardware set up (beam spacing, incidence angle, distance between sample and camera, etc.), but radii on the order of 2-5 km have been measured with the nominal test configuration.

Although not originally intended for this purpose, the data from the MOSS system can be reduced to yield local slope information on the sample to be used in estimating surface profile. This is done by recording the location of the reflected rays on the CCD camera and comparing them to the spot locations yielded by an optically flat reference sample. To illustrate, a single member of the laser array is shown in Figure 4-2 reflecting off a sample at location x_i. For a flat sample, the incident ray inclined at an angle α to the vertical will reflect off the surface along the dashed line, impinging on the detector plane at point A. If the sample is deformed with local slope θ_i as shown, then the reflected ray will deviate from the nominal path by an angle $2\theta_i$, encountering the detector at location B. The distance between the nominal and actual spot locations, Δ_i, is given by

$$\Delta_i = s_i \tan 2q_i \qquad \text{(eq 4.1)}$$

in which s_i is the distance between the sample and the detector along the nominal ray path. The spot migration can be related to the surface slope by first recalling the surface slope definition

$$u'(x_i) = -\tan q_i \qquad \text{(eq 4.2)}$$

and using the double angle trigonometric identities to yield

$$u'(x_i) = \frac{s_i}{\Delta_i} - \left[\left(\frac{s_i}{\Delta_i}\right)^2 + 1\right]^{1/2}. \qquad \text{(eq 4.3)}$$

In this development the spot migration resulting from a pure translation of the surface has been neglected. This effect, while negligible for the cases considered in this study, might be a significant source of error for samples undergoing large deformations. For such cases, a second measurement of the reflected ray is needed to distinguish the contributions of the sample slope and displacement to the spot migration. Such a measurement can be readily obtained using a beam splitter and a second CCD camera.

4.1.2 Surface Profile Estimation

Once the slopes are known at n discrete points on the sample surface, curve fitting algorithms can be used to estimate the distributed displacement profile. The approach taken here is to use cubic spline functions shown in Figure 4-3 to estimate the shape in the regions R_i between the data points. These functions take the general form

$$u(x) = a_i x^3 + b_i x^2 + c_i x + d_i, \forall x_{i-1} \le x \le x_i, i = 1,2,,...n+1 \qquad \text{(eq 4.4)}$$

in which u is the surface displacement and a_i, b_i, c_i, and d_i are the initially undetermined spline coefficients representing $4(n+1)$ unknowns. A unique solution to the profile is given by enforcing the $3n$ spline compatibility conditions (displacements, slopes, and curvatures are equal at the spline junctions), incorporating the n measured slopes, and imposing 4 boundary conditions at the sample end points.

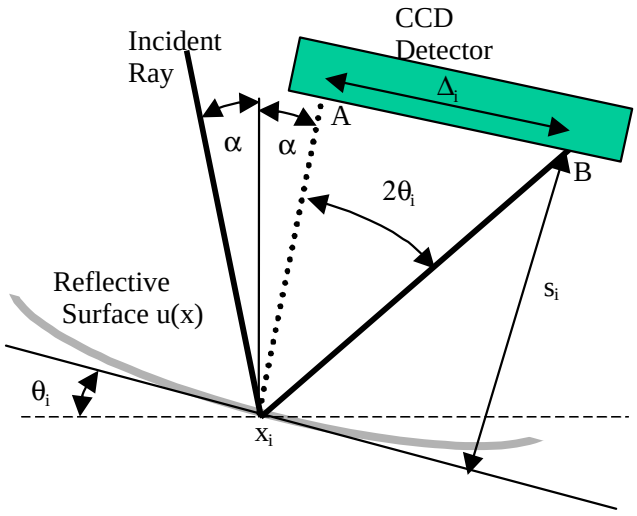

Figure 4-2. Ray-tracing diagram for demonstrating discrete slope measurements on sample surface.

To illustrate the curve fitting procedure, we first consider a 3 cm long sample clamped at the center and deformed in the shape of a perfect parabola with focal length of 2 m. The sample is interrogated with 6 evenly spaced parallel rays inclined at angle $\alpha = 10°$ relative to the vertical. The rays reflecting off the concave surface converge as they approach the CCD camera located 1 meter from the sample surface. The spot locations are recorded and compared to those of an optically flat sample. The resulting Δ_i's are used to estimate slope (according to equation 4.3) which are then used to produce the surface profile shown in Figure 4-4.

In the absence of surface errors and measurement noise, the six data points provide an exact fit to the surface. However, much more data may be needed to adequately represent the profile of a highly distorted surface. For example, consider a sinusoidal distortion superimposed on the parabolic profile of the previous example. The error curve with period 3.75 mm and amplitude of 1 mm produces small changes in the surface slope at the measurement locations. As shown in Figure 4-5, considerable errors are present in the profile estimated using only 6 discrete slope measurements. The error, however, is significantly reduced by the inclusion of additional data points. With 24 slope measurements, the general profile of the distorted surface is captured as indicated in the figure.

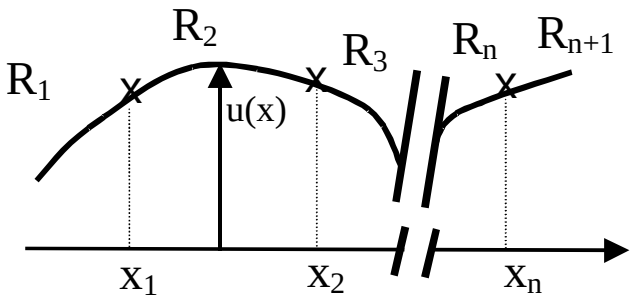

Figure 4-3. Cubic spline representation of sample surface.

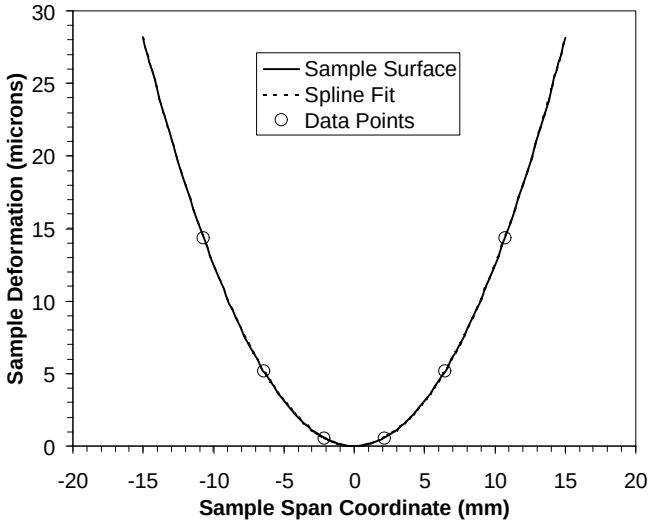

Figure 4-4. Surface profile estimation using cubic spline routine with 6 discrete slope measurements.

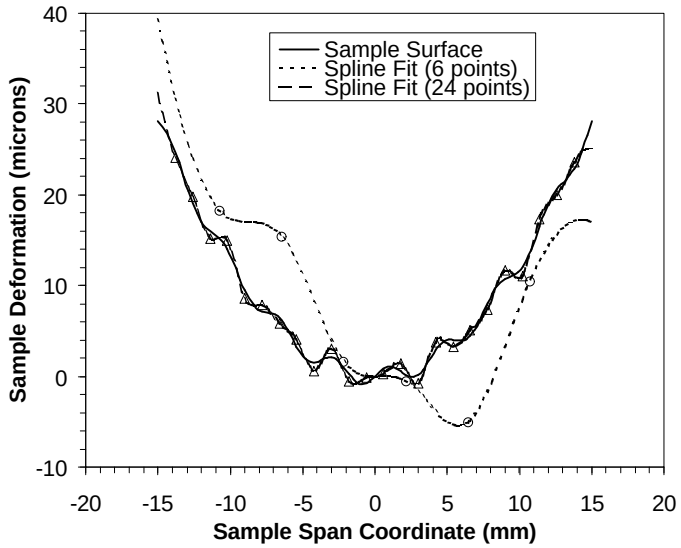

Figure 4-5. Profile estimation of distorted sample surface using 6 and 24 discrete data measurements**.**

Although the MOSS system's default configuration allows for only four discrete slope measurements, increased resolution can be obtained by altering the etalon to reduce the beam spacing, and stepping the sample underneath the beam array. This approach was taken in the following experimental investigation.

4.1.3 Experimental Demonstration of MOSS Based Profiler

To illustrate the utility of the proposed surface estimation procedure on a real sample, a series of experiments was conducted on a deformable piezoelectric actuator subjected to varying excitation levels. Morgan Matroc (model #61620) manufactured the PZT-5A bimorph actuator used in the experiment. Featuring parallel wiring and full nickel electrodes, the actuator had nominal dimensions of 5 x 2 x 0.06 cm. One side of the actuator was polished to obtain a sufficient level of reflectivity to enable interrogation by the MOSS system. In all of the experiments conducted, the actuator was clamped at one end, exposing approximately 3 cm in a cantilevered configuration. To simplify the connection of electrodes to the sample, only the upper plate of the bimorph was excited. With the bottom half of the actuator acting as a constraining layer, applying a potential across the upper plate caused a bending deformation that altered the path of the reflected beams. An array of four parallel beams with horizontal spacing of 1.4 mm and an incident angle of $\alpha = 2.5°$ were tracked by the CCD camera. At each excitation level, the sample was stepped under the beam array to provide additional data points. Depending on the degree of sample deformation, varying amounts of data were obtained before the reflected rays passed out of range of the stationary camera.

As shown in Figure 4-6, interrogation of the zero volt sample yielded twenty data points which were then used in the cubic spline surface profiler. Some initial distortion was present in the sample as a consequence of residual stresses induced in the fabrication and polishing procedures. Increasing the excitation level (positively) resulted in an upward curvature. Tip deflections of 30 and 50 μm above the zero volt reference were estimated for

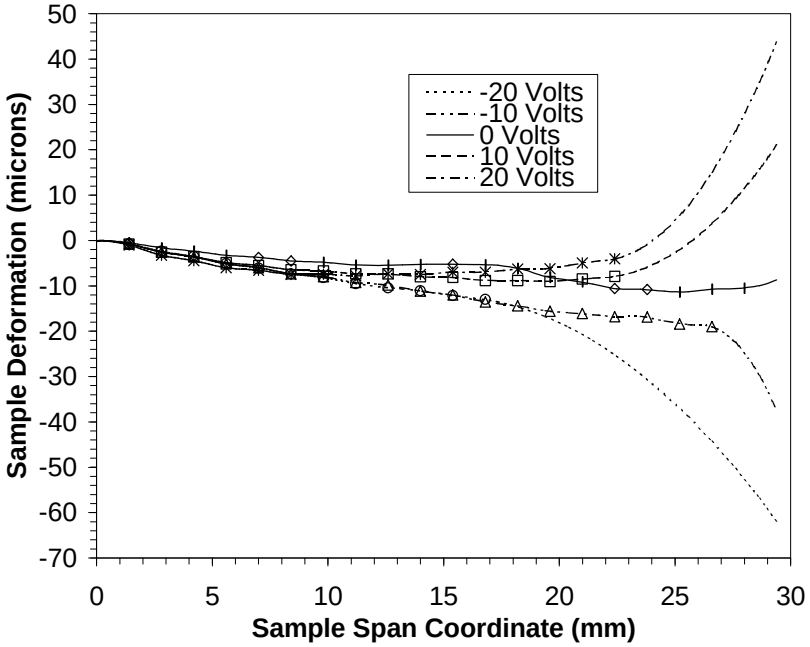

Figure 4-6. Profile estimation of sample surface at varying excitation levels**.**

the 10 and 20 volt cases, respectively. These estimates, however, were obtained using only 16 data points in the curve fitting procedure, since beam reflections on the outboard portion of the sample fell out of range of the CCD camera. Therefore, the profile in this region is an extrapolation from the last slope measurement available at x = 22.5 mm.

Negative excitations produced a downward curvature in the sample as anticipated. At -10 volts, 19 data points were used to obtain a relative tip deflection of -30 μm. The deflection estimate increased to -60 μm at -20 volts, though only 12 data points were available.

4.1.4 Summary of MOSS Results

While the existing MOSS system was suitable for demonstration purposes, several modifications are needed to realize the full potential of this approach for measuring sample deflections. In the experiment conducted, moderate excitation levels produced surface distortions sufficient to steer the beams out of the range of the detector. Therefore, a method for expanding the range of the slope measurement is needed to maximize the surface discretization. Moving the camera closer to the sample would expand it's range, but at the expense of resolution. Another approach yielding a similar result is to employ additional optical elements that steer the beam back onto the camera. Expanding the dynamic range requires a CCD camera with a larger sensing array. For even larger deformations, the camera could be mounted on a linear stage, enabling tracking of the reflected beams.

A second issue requiring additional consideration is that of slope errors resulting from surface displacements. As mentioned previously, migration of the reflected beams across the surface of the detector are attributed solely to changes in the surface slope. While this assumption is valid for small surface distortions, surface translations can produce beam

migrations that are indistinguishable from migrations resulting from steering the beams via slope changes.

4.2 Keyence Sensor

While the previously described technique is capable of profiling small samples with deflections on the order of a few tens of microns, a more robust system with increased range is needed to perform characterization studies on highly deformable films. A second coarse sensing approach considered was a Keyence LK-2500 laser displacement sensor mounted on a precision Newport stage system. The sensor is similar to the MOSS technique in that a laser is reflected off the mirror surface to measure surface displacements. The Keyence sensor provides for an absolute measure of the surface position at a single point. Full surface profiles can be obtained by a point-by-point scanning of the sample surface.

The LK-2500 CCD laser displacement system uses a triangulation measurement principle. A semiconductor laser beam is reflected off the target surface and passes through a custom designed receiver lens system. The beam is focused on a CCD sensing array. The CCD detects the peak value of the light quantity distribution of the beam spot for each pixel within the area of the beam spot and determines the target position. As the target displacement changes relative to the LK-2500 sensor head, the reflected beam position changes on the CCD array. These positional changes are analyzed by the LK-2500 Controller which resolves positional changes of 50 μm at distances of 250-750 mm. The Laser Time Flash Control (LFTC) facilitates this accuracy – regardless of target surface wetness, color or angle of orientation to the sensor. This large range (5 cm) and high resolution (50 μm) greatly improves the flexibility of the system over that of previous measurement techniques.

The LK-2500 includes a class II red semiconductor laser with a 0.3 mm visible beam spot that easily measures tiny targets and simplifies setup and alignment. Analog outputs of ±5 V, ±10 V and 4 to 20 mA may be specified. The LK-2500 can also perform detection into an enclosure through a glass window, as needed to interrogate electron gun controlled films mounted in a vacuum chamber. The laser displacement sensor is capable of sampling at 977 Hz, and can therefore be scanned rapidly over a sample to completely map the surface.

To enable surface profiling, the LK-2500 Keyence sensor was placed on precision Newport Translation stages that have a positional accuracy of 0.1 μm. The stages were programmed to scan the Keyence sensor in 1 mm steps across the bimorph mirror to obtain a surface profile. This profiling system was used to calibrate the change in the mirror shape as a function of electron gun energy and bimorph mirror electrode potential. It has also been used to provide real time tip displacement in a closed-loop shape control experiment.

Figure 4-7 shows the Keyence sensor on the Newport translation stages. The Keyence measured the surface profile of the bimorph mirror inside of the vacuum chamber shown in Figure 4-8. The mirror is approximately 5 cm X 10 cm in size and is held clamped on one side, but free to move otherwise.

Complete sets of data were taken for bimorph mirrors with various electrode materials. The mirror profile was measured for various electron gun energies and electrode potentials. This was done to calibrate the interaction of the electron gun with the various bimorph mirrors and to determine the optimal gun energy level to use in the system. These data cubes form the foundation of the input-output models needed to develop model based shape control algorithms.

Figure 4-9 shows a three dimensional plot of the displacements produced in the bimorph mirror shown in Figure 4-8 when excited with a uniform electron beam at 800 eV energy and 600 volt electrode potential compared to a zero volt excitation. The tip of the mirror displaces approximately 0.64 mm at a radius of 68 mm from the clamped end. This causes a net change in the radius of curvature of the surface of approximately 3600 mm from the zero volt position. This demonstrates that large shape changes may be initiated with electron gun excitation when the bimorph mirror is softly constrained.

Figure 4-7. Keyence Sensor mounted on the Newport translation stage system.

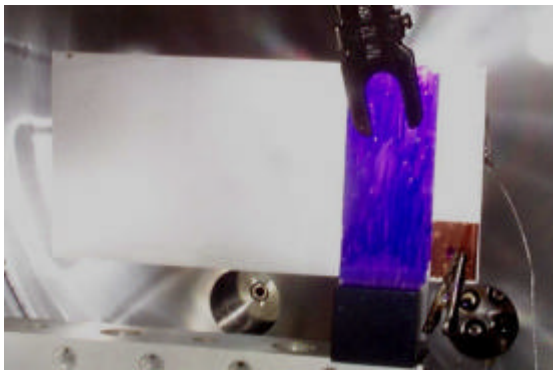

Figure 4-8. Piezoelectric bimorph mirror cantilevered from mount in vacuum chamber.

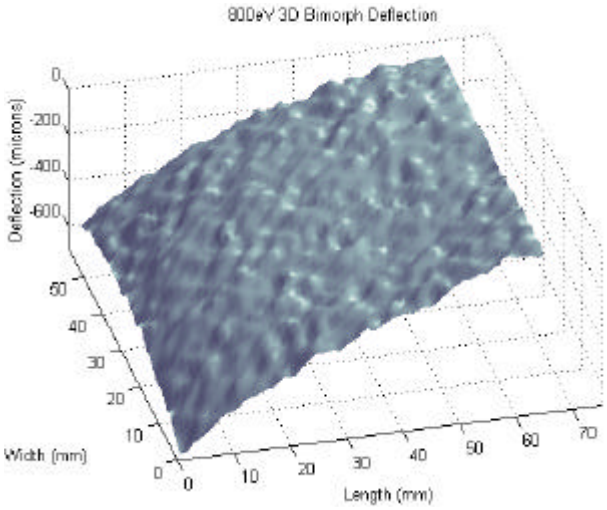

Figure 4-9. Shape change induced in bimorph mirror with electron gun excitation with 800 eV electron energy and a 600 volt electrode potential. The far right hand side of the mirror is the fixed end.

4.3 Interferometric Measurement Techniques

While the previous measurement systems are suitable for many tasks such as material response characterizations or control algorithm development, obtaining optical accuracy from a deployable mirror requires a much higher resolution sensing system. Traditional optical sensors such as interferometers and wavefront sensors have the required resolution but lack the dynamic range needed for this application. With traditional interferometry the number of fringes created across the surface is proportional to the deviation of the surface from the desired surface shape and the wavelength of light used in the measurement. Since the deployed mirror in its initial state will be orders of magnitude from its desired shape, the surface becomes impossible to resolve and analyze. We are utilizing two non-traditional interferometric techniques to measure the mirror surface profile. The first is electronic speckle pattern interferometry. This technique will give us a differential surface profile, but with modification may give us an absolute profile of the surface. The second is multi-wavelength heterodyne interferometry, which has the potential to give us a very accurate absolute surface profile with a large dynamic range.

4.3.1 Electronic Speckle Pattern Interferometry

Electronic Speckle Pattern Interferometry (ESPI) has been under development at Sandia by Bruce Hansche and Mike Valley. ESPI is essentially a video-based holographic interferometry device, which generates a "wrapped phase" image as its raw data output. That is, for a reference object position $Z_R(x,y)$, and a displaced object $Z_D(x,y)$ illuminated with wavelength l, the image produced is

$$I(x,y) = Kd(x,y)_{\mathrm{mod}(2p)} \qquad \text{(eq 4.5)}$$

where

$$d(x,y) = (4p / l)(Z_D(x,y) - Z_R(x,y) \qquad \text{(eq 4.6)}$$

and K is an intensity scaling constant. This equation assumes illumination and viewing directions essentially normal to the displacement direction.

The wrapped phase image must be "unwrapped" by adding multiples of 2π at the "wrap boundaries". This process converts $d(x,y)_{\mathrm{mod}(2p)}$ to a continuous $d(x,y)$. Multiplying by $\{(4\pi/\lambda)/K\}$ converts the continuous phase map to a deformation map.

There are several advantages to this approach over the other measurement techniques considered. For example, the mirror surface can be essentially any shape since measurements are referenced to the initial shape and not an ideal shape. In addition, ESPI is a whole-field technique, allowing measurement of the entire surface simultaneously. Finally, this approach offers very high sensitivity, measuring deflections on the order of 100 nm easily with a theoretical limit approaching 1 nm. This technique has greatly aided in studying surface shape changes initiated by electron gun excitation. Some significant limitations of ESPI are that it only works well with diffuse surfaces, and in its current

configuration it can only provide relative surface deflections as opposed to absolute measurements. With some alterations, ESPI may be used to measure absolute profiles, but the required modifications are beyond the scope of this program.

To illustrate the performance of the ESPI system, a number of samples were interrogated. First, the bimorph mirror was measured with the ESPI system after 30 seconds of electron gun excitation with an 800 eV uniform beam and a 2 V electrode potential. It was measured with the ESPI system again after an additional 30 seconds of electron gun excitation. Figure 4-10 shows the first interferogram taken of the bimorph mirror surface and one taken after an additional 30 seconds of electron gun excitation. The left edge of the thin-skin mirror is the clamped edge. The circular fringe near the clamped edge has gone from dark to light, indicating a change in shape on the order of 150nm. This result verifies the ability to effect miniscule surface changes with the electron gun as needed to achieve optical quality.

A second group of ESPI measurements were taken from a circular thin sheet of a piezoelectric co-polymer material clamped around the edges as shown in Figure 4-11. Since the in-plane piezoelectric coefficients are nearly identical in a co-polymer, the initially flat constrained material will assume a convex or concave shape in the presence of an electric field. An 800 eV electron beam was imposed on the material as the electrode potential was varied from -10 to +10 volts. The material displaced in a convex shape for positive voltages and a concave shape for negative voltages. The maximum deflection in the center of the material was approximately 200 nm for the 1 V electrode potential, 600 nm for the 5 V electrode potential, and 1300 nm for the 10 volt electrode potential. The resulting co-polymer material shape is shown in Figure 4-12 for ± 5 V and ± 1 V excitation force.

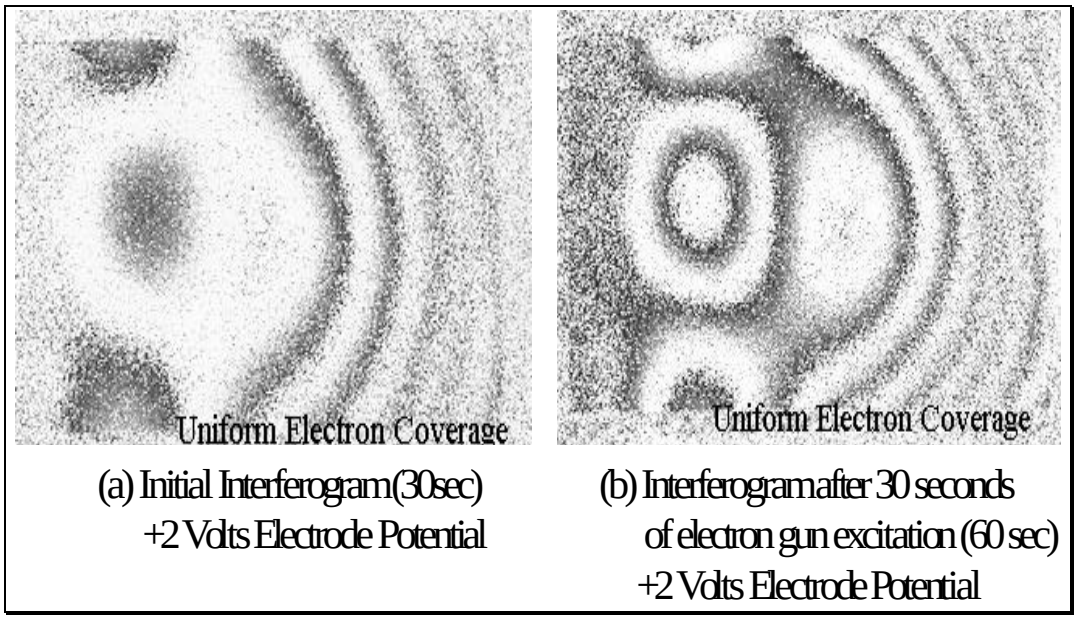

Figure 4-10. Interferograms of bimorph mirror with electron gun induced shape changes, clamped end on left**.**

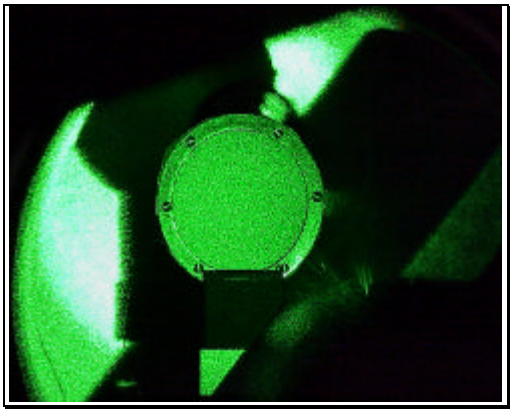

Figure 4-11. Co-polymer piezoelectric thin-skin in ring clamp**.**

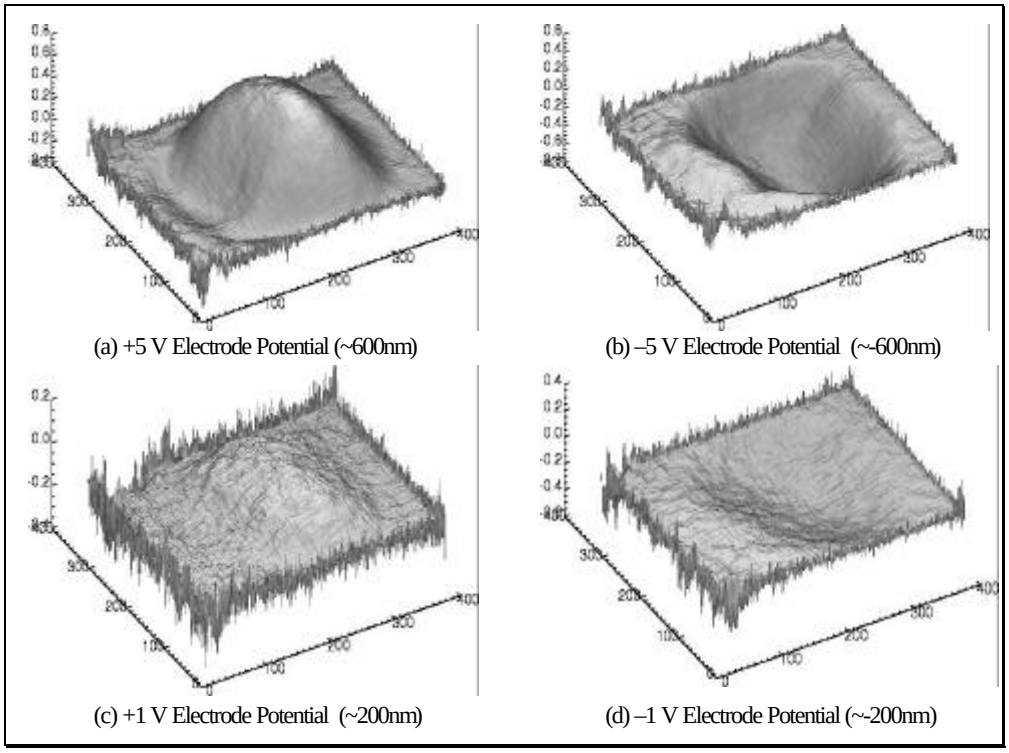

Figure 4-12. Co-polymer shape change as a function of electrode potential for an 800 eV electron gun excitation**.**

4.3.2 Multi-Wavelength Heterodyne Interferometry

An interferometric measurement technique that shows great promise for delivering both the necessary sensitivity and dynamic range for deployable thin-skin mirror applications was recently under development at Air Force Research Laboratories (McMakin et al, 1997 and Voelz et al., 1997). This approach takes advantage of an optical beating phenomenon to synthesize long wavelength interferometry ideal for profiling highly distorted surfaces. Multi-wavelength heterodyne interferometry creates an interferogram at two different wavelengths with a tunable laser, then creates an interferogram in the software at a synthetic wavelength given by

$$l_s = \frac{l_1 l_2}{l_1 - l_2}, \qquad \text{(eq 4.7)}$$

where λ_s is the synthetic wavelength, and λ_1 and λ_2 are the original wavelengths (McMackin et al., 1997, 1998). The synthetic wavelength can be much larger than the actual wavelengths, yielding only a few fringes across a highly distorted surface. Furthermore, measurements can be taken at many different wavelengths and various wavelength pairs can be chosen to provide a wide range of synthetic wavelengths and tunable accuracy. Large synthetic wavelengths accurately profile large surface deviations or discontinuities at low sensitivity, while smaller synthetic wavelengths profile small deformations with high surface measurement accuracy. This technique can potentially provide the 4 to 5 orders of magnitude dynamic range and 25 nm surface measurement accuracy needed for profiling large deployable space optics.

A cooperative effort was established with the Air Force Research Lab (AFRL) to provide surface profiles of PZT bimorph wafers using the AFRL multi-wavelength heterodyne interferometry system shown in Figure 4-13. Figure 4-14 shows an interferogram utilizing a synthetic wavelength of approximately 10 μm when the sample is subjected to a 10V excitation. Further evaluation of this sensing technique for a thin-skin mirror will continue provided an additional agreement can be worked out with AFRL.

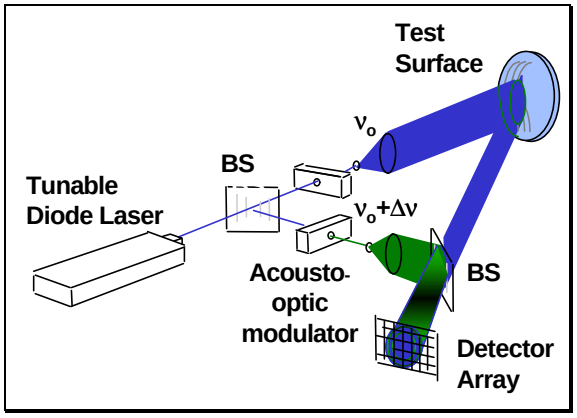

Figure 4-13. AFRL multi-wavelength heterodyne interferometry system.

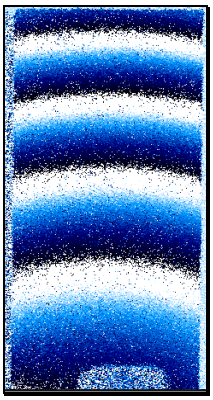

Figure 4-14. Interferogram of a PZT bimorph with 10 V excitation taken with a synthetic wavelength of 10 μm.

5. ELECTRON GUN EXPERIMENTAL RESULTS

A polyvinylidene fluoride (PVDF) bimorph was chosen to perform the function of a shape-controlled thin-skin mirror for this research. The PVDF actuator was constructed from a two-layer bimorph as seen previously in Figure 2-1. The mirror is mounted in a cantilever fashion. In this manner the flexure of the cantilever beam approximated the curvature that would be seen in a cylindrical mirror. The curvature of the mirror was then adjusted by controlling the electric field across its thickness. In this experiment the field is the result of the potential on the bare side as manipulated by the electron gun and the potential of the mirror/electrode.

5.1 Bimorph Mirror Calibration

Bimorph mirrors have been fabricated and placed into the vacuum chamber with the electron gun. To move toward a complete understanding of electron gun control of piezoelectric bimorph mirrors, a system for precise surface mapping was developed as discussed in the previous chapter. This system provides "real-time" feedback for the use of closed-loop control, as well as the ability to resolve a wide range of surface deflections with an extremely high resolution. To that end optical tests were conducted with the Keyence sensor to determine the surface profile of the mirrors and how they change with electron gun excitation.

The Keyence sensor was tested by applying a voltage across a bimorph using a direct current (DC) power supply and measuring its deflection. A simple feedback system was programmed with LabView to evaluate the Keyence sensor. The sensor was then integrated with the electron gun control program to measure the deflection of a bimorph while it was in the vacuum chamber being controlled with the electron gun. Since the Keyence sensor provides measurement of deflection at only a single point, it was integrated with a two-dimensional x-y motion translation stage to provide scanning of the sensor over the bimorph surface. The stage is capable of motions of 100 nm. The system was controlled with a general-purpose interface bus (GPIB) controller to aid in closed loop measurements.

A very detailed calibration of the bimorph mirrors was completed. The change in the bimorph mirror surface shape as a function of electron gun energy and electrode potential was carried out. This was completed for several bimorph mirrors with varying electrode materials and configurations. Figures 5-1 through 5-8 represent a sample of this data for a NiCu mirror with an opposing bare face, and a NiCu mirror with an opposing NiCu face. The opposing faces are toward the electron gun.

The optimum beam energy was determined through the use of deflection optimization (Figures 5-1 through 5-8) and hysteresis plots for both the NiCu-Bare PVDF (bare) configuration and the NiCu-NiCu (dual metal) configuration. From Figure 5-4 it can be seen that the most efficient energy level for the bare mirrors is 800eV. Figure 5-8 shows that 600eV is the most efficient energy level for the dual metal mirrors.

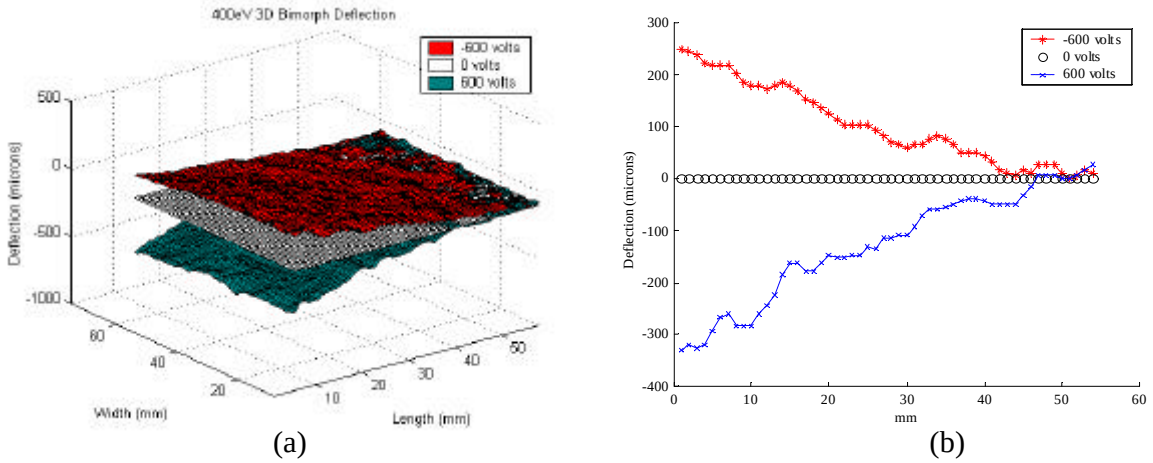

(a) (b)

Figure 5-1. NiCu-Bare bimorph shape deformation comparison with centerline plots for ±600 volt electrode potential with a 400eV electron gun excitation**.**

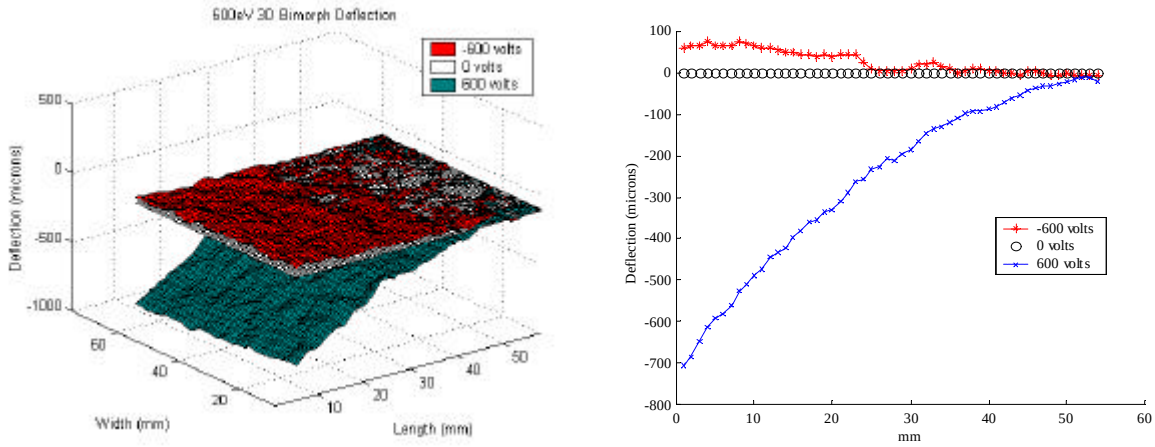

(a) (b)

Figure 5-2. NiCu-Bare bimorph shape deformation comparison with centerline plots for ±600 volt electrode potential with a 600eV electron gun excitation**.**

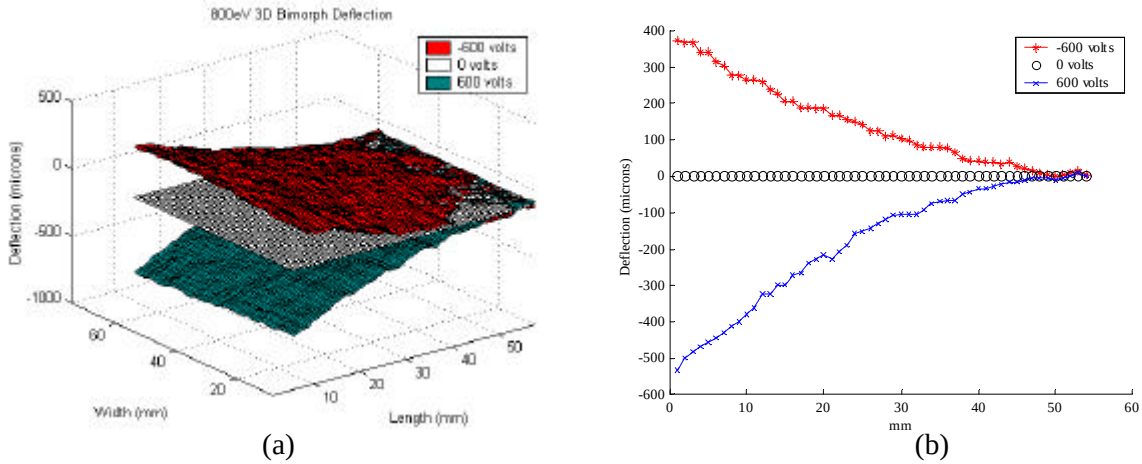

(a) (b)

Figure 5-3. NiCu-Bare bimorph shape deformation comparison with centerline plots for ±600 volt electrode potential with an 800eV electron gun excitation**.**

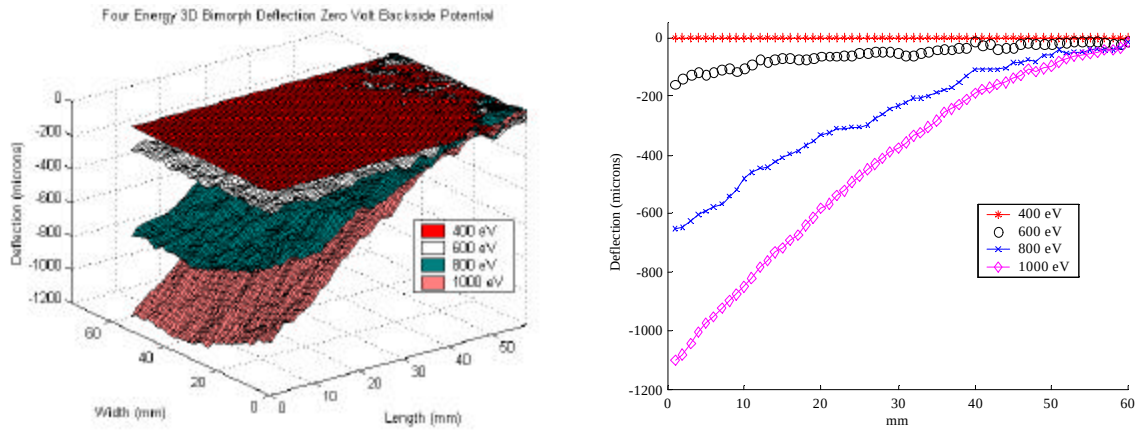

(a) (b)

Figure 5-4. NiCu-Bare bimorph shape deformation comparison with centerline plots for a zero volt electrode potential with a 400, 600, 800, and 1000eV electron gun excitation**.**

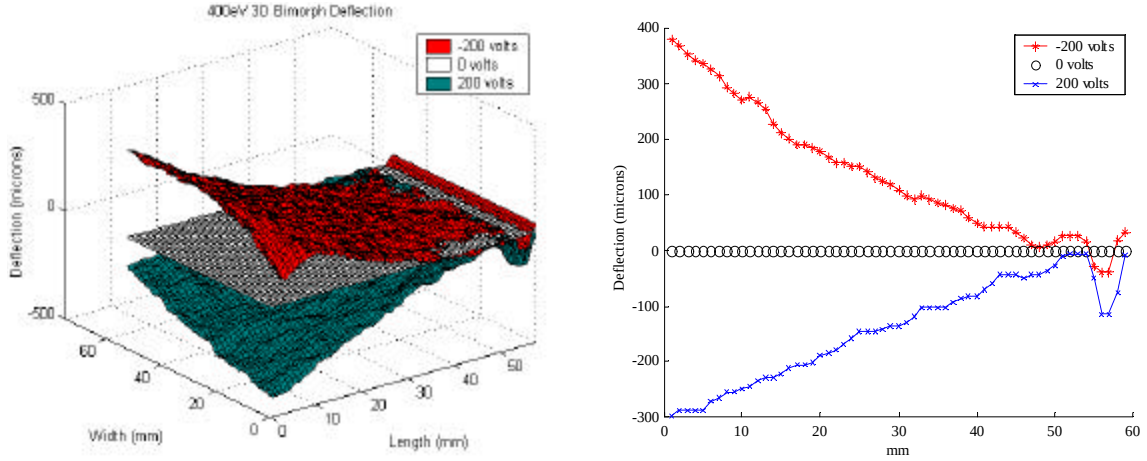

(a) (b)

Figure 5-5. NiCu-NiCu bimorph shape deformation comparison with centerline plots for ±200 volt electrode potential with a 400eV electron gun excitation**.**

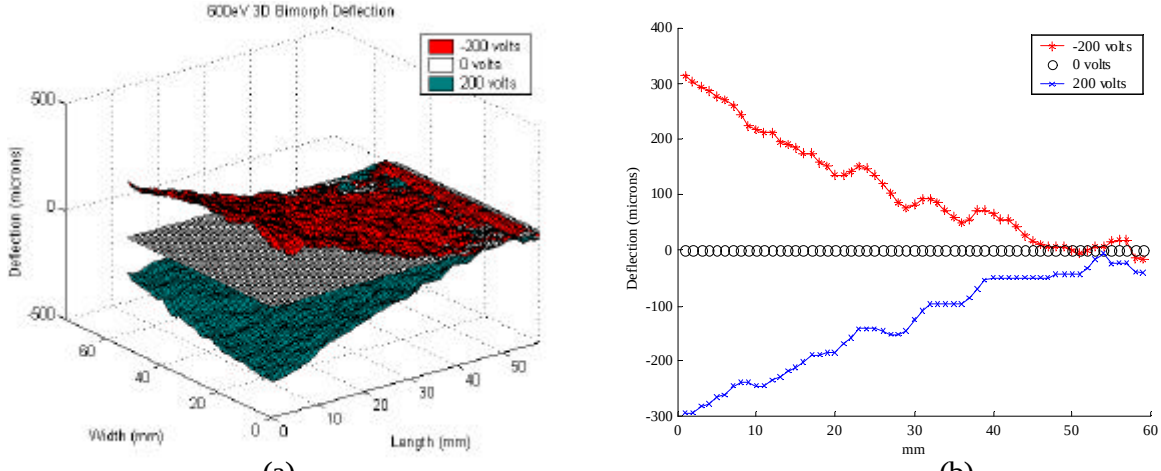

(a) (b)

Figure 5-6. NiCu-NiCu bimorph shape deformation comparison with centerline plots for ±200 volt electrode potential with a 600eV electron gun excitation**.**

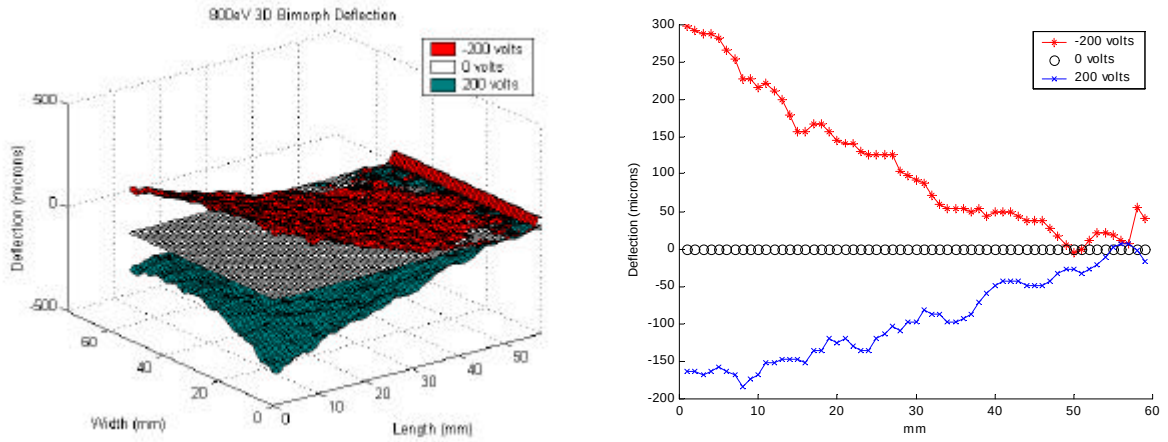

(a) (b)

Figure 5-7. NiCu-NiCu bimorph shape deformation comparison with centerline plots for ±200 volt electrode potential with an 800eV electron gun excitation**.**

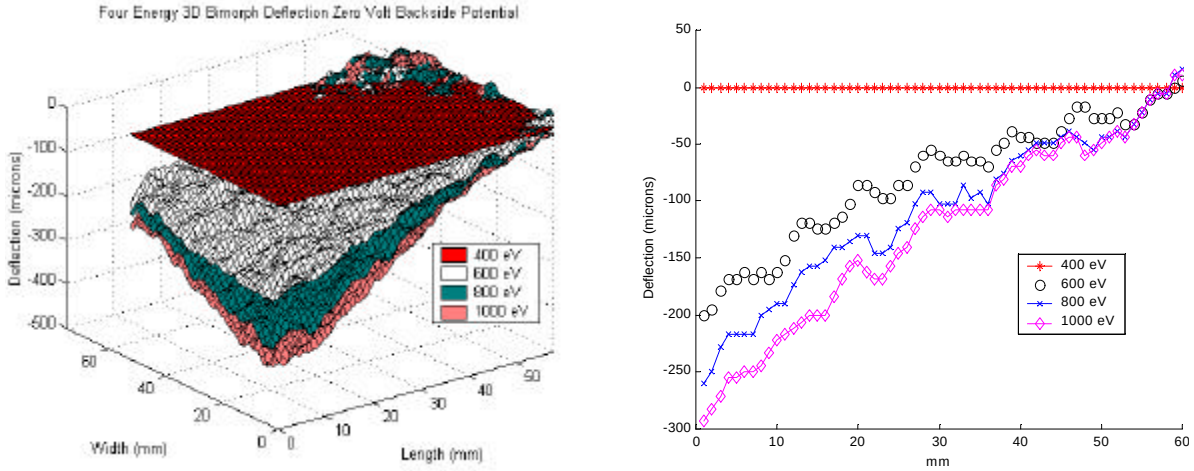

(a) (b)

Figure 5-8. NiCu-NiCu bimorph shape deformation comparison with centerline plots for a zero volt electrode potential with a 400, 600, 800, and 1000eV electron gun excitation**.**

Figure 5-9 and Figure 5-10 represent the hysteresis in the mirror deflection versus electrode potential at the several energy levels for the bare configuration and the dual metal configuration respectively. It can be seen that the hysteresis found in the bare configuration is much less than that of the dual metal configuration. In Figure 5-10 a bifurcation occurs in the dual metal deflection curve. This is based on the material's secondary electron emissions (Section 2). This induces a shift in the optimum energy from configuration to configuration as seen from these figures. In this case for the dual metal mirrors it can be seen that Figure 5-10d has no bifurcation, and therefore the optimum energy turns out to be 1000eV.

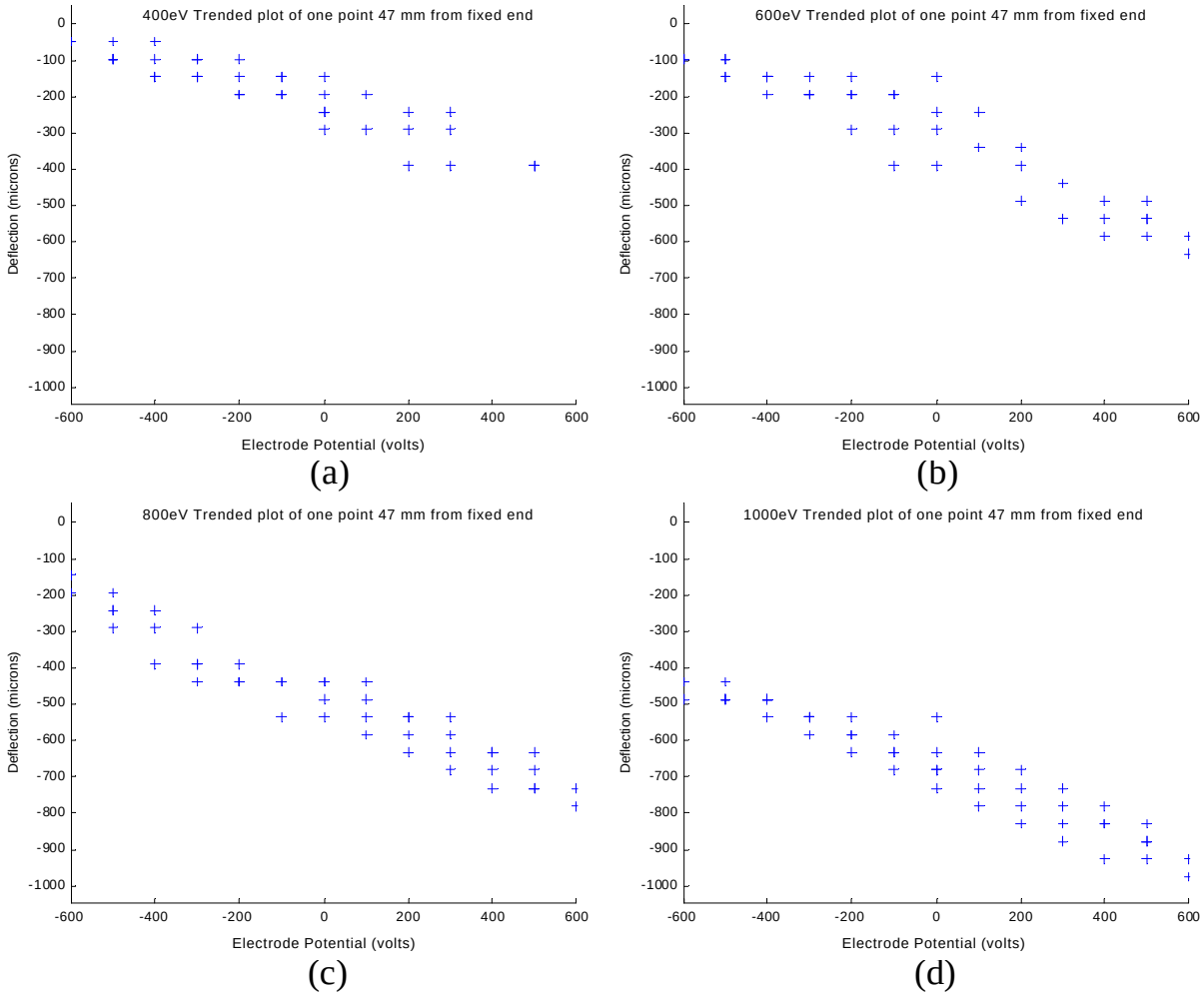

Figure 5-9. Hysteresis for NiCu-Bare PVDF electrode configuration at 400, 600, 800, and 1000eV**.**

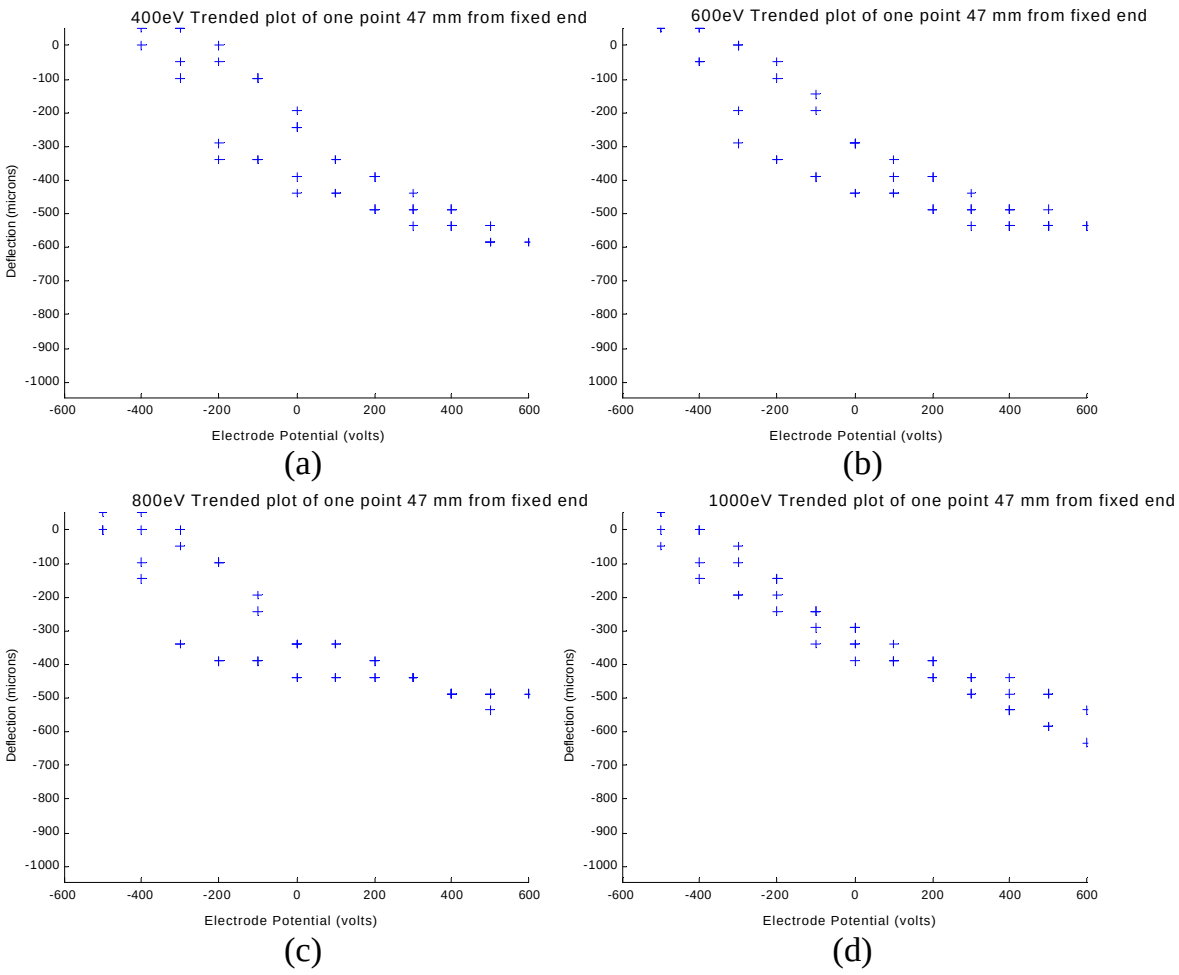

Figure 5-10. Hysteresis for NiCu-NiCu PVDF electrode configuration at 400, 600, 800, and 1000eV**.**

5.2 Closed-Loop Mirror Shape Control

The shape control algorithms and electron gun control methods have been developed and tested in a closed-loop feedback system. After the bimorph mirror shape changes had been calibrated as a function of electron gun energy and electrode potential, a simple shape control algorithm was developed to control the deflection of the bimorph mirror at it's tip position. We used the Keyence sensor to measure the initial position of the tip of the mirror, and then the proportional integrator derivative (PID) control algorithm calculated the excitation profile necessary to induce changes to the tip position through electron gun excitation. This controller gradually incremented the tip location to the desired position within the dynamic range of the bimorph.

The position of the mirror tip was then continuously monitored and the control voltage adjusted to maintain the mirror tip in the new desired position. Any disturbances in the system were constantly balanced through electron gun excitation until a new tip position was commanded. This confirmed our ability to control the shape of the mirror tip in a closed-loop fashion and also validated that the calibration of the materials was done correctly. Figure 5-11 shows the time history of the mirror tip position experiment. In each case on the

far left hand side of the Keyence curve we see the mirror starting position and the progression to the desired position. In both plots the period of time from disturbance to equilibrium was approximately 5 to 10 seconds. It can easily be seen that once the mirror is at the desired position it is maintained there in a closed-loop fashion with the PID controller updating the position to consistently maintain stability even through possible disturbances.

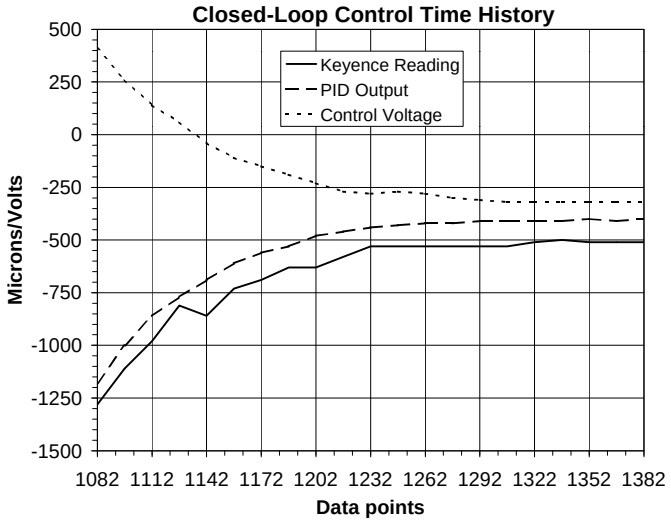

(a) closed-loop tip control at the first commanded position

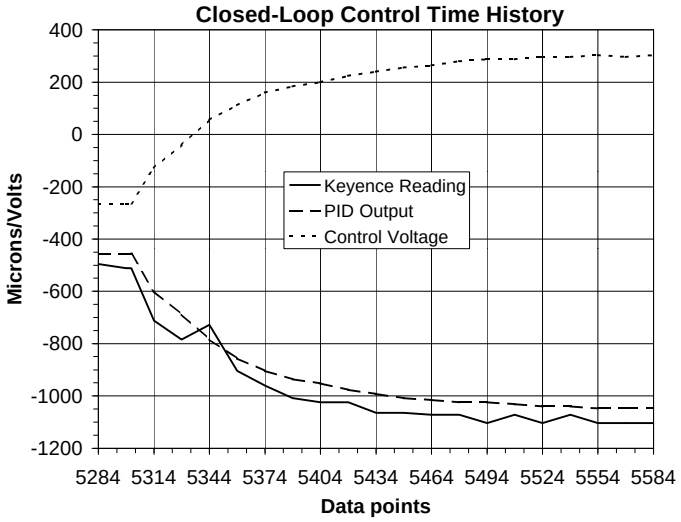

(b) closed-loop tip control at the second commanded position

Figure 5-11. Mirror tip deflection closed-loop control demonstration. The Keyence reading shows the position of the bimorph tip as a function time**.**

This page intentionally left blank.

6. SHAPE CONTROL ALGORITHMS

Quasi-static open-loop control algorithms suitable for reshaping bimorph mirrors have been investigated using finite element modeling techniques. Temperature sensitive layered shell elements in Abaqus were adapted to mimic the behavior of piezoelectric bimorphs. One-dimensional shape correction was first developed using the analytical bimorph equations to convert measured surface curvature errors to a corrective excitation profile. Extensions of this algorithm to two-dimensional curvature correction on a bimorph plate was accomplished using modeling derived curvature-voltage sensitivity matrices and allowing for electron gun excitation on both sides of the bimorph (Redmond et al., 1999). However, the impracticality of two-sided control in a space application led to the improvisation of a one-sided control algorithm based on modeling derived displacement-voltage sensitivity matrices. Each of these algorithms are summarized in this section and demonstrated on a finite element model of PZT-5A bimorph subjected to arbitrary disturbances.

6.1 One-Dimensional Shape Correction

Neglecting the effects of the relatively thin glue layers and electrodes, the internal moment resulting from excitation of a uniform PZT bimorph beam is given by (Martin et al., 1998)

$$\mathrm{M(x)} = \int_{-t/2}^{0} e_{31} E_3(x) bz \, dz - \int_{0}^{t/2} e_{31} E_3(x) bz \, dz \qquad \text{(eq 6.1)}$$

in which b and t are the beam width and thickness, z is the distance from the neutral axis, e_{31} is the piezoelectric field constant, and $E_3(x)$ is the axially distributed electric field. Assuming parallel wiring (ground plane at center) and separating the elastic and piezoelectric coefficients, the moment reduces to

$$M(x) = Y d_{31} b \frac{t}{2} V(x) \qquad \text{(eq 6.2)}$$

in which Y represents Young's modulus, d_{31} is the more familiar piezoelectric voltage constant, and $V(x)$ is the voltage difference between the outer surfaces and the center ground plane.

The corrective action of the PZT is superimposed on the deformation of the structure resulting from mechanical disturbances. For a uniform beam, the moment yields a corrective curvature according to

$$u''(x) = \frac{M(x)}{YI}, \qquad \text{(eq 6.3)}$$

where I is the area moment of inertia of the beam cross section ($I=bt^3/12$). Recognizing that the desired curvature correction is the difference between the desired curvature $u_d''(x)$ and the measured curvature $u_m''(x)$, equating Equations 6.2 and 6.3 yields

$$V_c(x) = \frac{t^2}{6d_{31}}(u_d''(x) - u_m''(x)) \qquad \text{(eq 6.4)}$$

in which $V_c(x)$ is the distributed corrective excitation profile.

6.2 Two-Dimensional Shape Correction

Practical optical applications such as remote sensing require controlling surface curvature in two directions in order to achieve complicated profiles such as a paraboloid from a general initial profile. This can only be achieved with two linearly independent controls. This is difficult to realize in practice since both x and y curvatures are generally induced by a single excitation across the thickness of the piezoelectric material. One possible solution, which requires independent excitation of the top and bottom layers of a bimorph structure, is now presented. A second approach in which voltage-displacement sensitivities are manipulated to make coarse corrections with one-sided control is presented in a later section.

The relationship between curvatures and the excitations at a point on a bimorph structure involve a complex coupling of the electromechanical properties of the piezostructure. A general linear model is expressed as

$$\begin{bmatrix} g_x(x,y) \\ g_y(x,y) \end{bmatrix} = \begin{bmatrix} F_t(x,y) & F_b(x,y) \\ G_t(x,y) & G_b(x,y) \end{bmatrix} \begin{bmatrix} V_t(x,y) \\ V_b(x,y) \end{bmatrix}, \qquad \text{(eq 6.5)}$$

in which γ_x and γ_y are the curvatures along the x and y directions, V_t and V_b are the top and bottom surface excitations, and F and G are the coupling coefficients. Although the coupling coefficients naturally vary over the surface due to slight variability in the structural and material properties, they are nominally the same for materials displaying uniform piezoelectric properties ($d_{31} = d_{32}$). Therefore, excitation of the top or bottom surface will produce similar curvature changes in both the x and y directions. In this case, the coefficient matrix of Equation 6.5 is singular, and it is not possible to determine a corrective excitation profile to negate general curvature errors.

To circumvent this difficulty, we allow the bimorph to consist of a preferentially biased material such that $d_{31} \neq d_{32}$, an effect that can be achieved by straining the material during poling. Then, offsetting the layers of the bimorph by 90 degrees renders the coefficient matrix of Equation 6.5 nonsingular. Top and bottom surface excitation profiles can then be uniquely determined for general curvature corrections. One approach to achieving independent excitation of the top and bottom layers of the bimorph using a single electron gun is illustrated conceptually in Figure 6-1. Small holes are included in the top layer to provide access to the bottom layer. Other possibilities include making the top layer

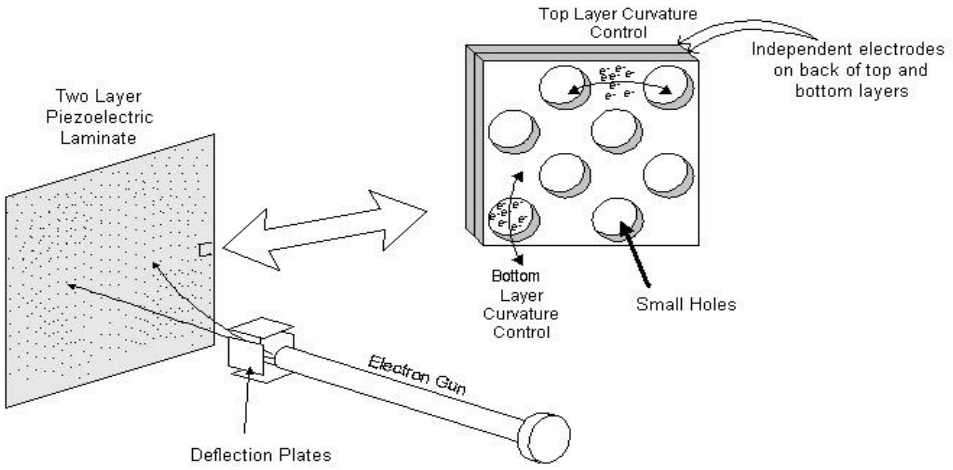

Figure 6-1. Conceptual design for a bimorph mirror amenable to independent layer control using a single electron gun excitation source**.**

transparent to particular energy levels, allowing the electron stream to pass through unabated to the backside.

For a uniform structure, the coefficient matrix of Equation 6.5 can be determined analytically, but an experimental calibration procedure is favored to accommodate probable uncertainties in material and fabrication parameters. Furthermore, nonlinear behavior can be captured by including additional higher order terms in Equation 6.5, which can be quantified in the same way using additional excitation levels. A linear calibration procedure is illustrated in the second of the following examples.

6.3 Shape Correction Illustrations

The quasi-static shape correction algorithms presented in the previous pages are now illustrated on a series of examples. Layered shell elements in the Abaqus (Hibbitt et al., 1998) finite element modeling package were adapted to mimic the behavior of piezoelectric bimorph ceramics subjected to both external disturbances and electric field loading. Each example required numerous iterations between the modeling package and the control algorithms. The process was automated in the Matlab (The Mathworks, 1999) programming environment which made needed calls to retrieve the finite element analysis results, process the data, generate new input decks, and then execute a subsequent modeling run.

6.3.1 Cantilevered Bimorph

We first consider a cantilevered PZT-5A bimorph beam whose parameters are summarized in Table 6-1 (Morgan Matroc, 1993). A layered shell model was subjected to initial disturbances yielding the error shape shown in Figure 6-2a. For this example, a constant curvature of 0.001 cm^{-1} along the beam span is desired. The element strains on the upper surface were interpolated to nodal strains and converted to curvature measurements according to

$$u_m''(x) = \frac{e_{11}^{top}(x) - e_{11}^{bot}(x)}{t} \qquad \text{(eq 6.6)}$$

in which t is the bimorph thickness and ε_{11}^{top} and ε_{11}^{bot} are the axial strains on the top and bottom surfaces.

From Equation 6.4, the corrective excitation profile for the top surface was determined as shown in Figure 6-2b. For this one-dimensional example, it is sufficient to show the single profile with the implicit assumption that a similar profile of opposite polarity is applied to the bottom surface. Then, a second finite element analysis exercising the electromechanical coupling of the piezoelectric with the corrective excitation profile was completed, yielding the corrected profile shown in 6-2c.

Although the control algorithm illustrated in this example provides useful insight into the shape correction methodology, it is ill suited to the general problem of mirror shape control. The algorithm cannot correct for an arbitrary disturbance due to its one-dimensional structure, and its reliance on an analytical model for determining corrective voltage makes it difficult to achieve optical quality surfaces in the presence of material and structural uncertainty.

Table 6-1. Sample parameters for one-dimensional cantilevered bimorph example.

Material	PZT-5A
Dimensions	20x4x0.06 cm
d_{31}	-171×10^{-12} m/V
d_{32}	0 m/V
Young's Modulus	6.1×10^{10} N/m^2
Wiring	Parallel
Desired Curvature	0.01 cm^{-1}

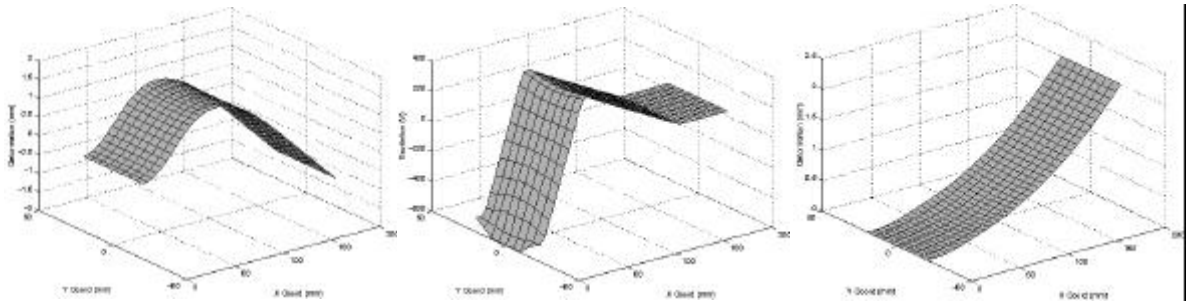

a. initial deformed shape b. corrective excitation profile c. final parabolic shape

Figure 6-2. One-dimensional shape control illustration using a distributed excitation source on a cantilevered PZT bimorph beam**.**

6.3.2 Two-Sided Excitation of a Bimorph Plate

Circumventing the shortcomings of the one-dimensional algorithm, a two-dimensional algorithm is now developed using a calibration procedure for determining the appropriate coupling coefficients. A finite element model of a square bimorph plate with parameters summarized in Table 6-2 was fixed at its center point and subjected to an arbitrary loading.

The resulting deformed profile is shown in Figure 6-3a, revealing a curvature error representative of the general mirror problem. The distributed coupling coefficient functions of Equation 6.5 were determined by applying uniform voltages to the top and bottom surfaces of the deformed structure and extracting the curvature sensitivities. This procedure mimics the calibration step to be implemented in future experiments. The corrective voltages needed to obtain the desired curvature of 0.004 cm^{-1} at each node point were calculated by multiplying the curvature error present in the initial deformed structure by the inverse of the local coefficient matrix. The resulting top and bottom surface excitations are shown in Figure 6-3b, revealing significant variation in the profiles, particularly in the vicinity of the fixed center point. A final finite element solution exercising the piezoelectric properties of the model was computed, yielding the corrected profile shown in Figure 6-3c. Only minor discrepancies in the corrected profile are evident and can be attributed to the relatively coarse discretization of the surface in comparison to actual electron gun spot size.

Table 6-2. Parameters used in two-sided actuation example of a PZT-5A bimorph wafer.

Material	PZT-5A
Dimensions	10x10x0.06 cm
d_{31}	-171×10^{-12} m/V
d_{32}	-57×10^{-12} m/V
Young's Modulus	6.1×10^{10} N/m^2
Wiring	Parallel
Desired Curvature	0.004 cm^{-1}

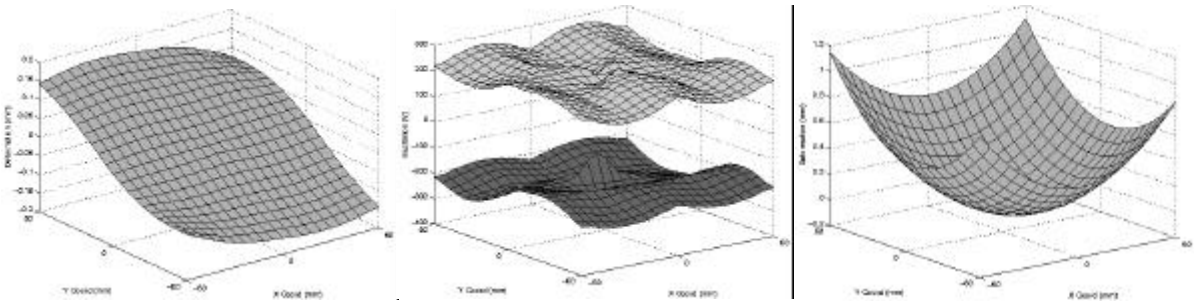

a. initial deformed shape b. corrective excitation profile c. final parabolic shape

Figure 6-3. Two-dimensional distributed shape control illustration using a distributed excitation source on a square PZT-5A bimorph plate featuring preferential layer deformations and independent layer control**.**

6.3.3 One-Sided Excitation of a Bimorph Plate

While correcting the curvature in two directions at each point requires independent control of each layer of the bimorph, a one-sided control can be improvised for a discrete number of points on the sample surface. This approach is well suited for initial shaping experiments in that it relies on segmented electrodes on the electron gun side of the sample. As opposed to direct incidence of the electron beam on the bare face of the wafer, the segmented electrode provides a precise target for the gun and yields a well-defined excitation region. Furthermore, this problem can be formulated as a uniquely determined or over determined inverse problem in which the goal is to place several distinct points of the sample on a desired surface.

To illustrate the approach, a 10 cm square wafer shown in Figure 6-4 is patterned with a 4 x 4 grid of electrodes and fixed at its center point. The thickness of the electrodes was ignored in this example and the material parameters were identical to those given in Table 6-2. As opposed to the voltage-curvature sensitivities determined in the previous example to define Equation 6.5, a 16 x 16 matrix relating electrode voltage to electrode mid point displacements was determined through sequential excitation. Linear deformations were assumed in this example, but nonlinear sensitivities could be captured using additional excitation levels.

Once the voltage-displacement sensitivities were known, the plate was deformed by applying a checkerboard pattern of 0.05 Newton discrete loads at the electrode centers. The resulting deformation is shown in Figure 6-5a, illustrating the expected saddle shape of the plate. For this example, it was decided to place the 16 electrode centers on a paraboloidal surface with x and y curvatures of 0.002 cm^{-1}. This is accomplished by inverting the uniquely determined sensitivity matrix to yield the corrective electrode excitation profile shown in Figure 6-5b. The resulting wafer profile is shown in Figure 6-5c, in which the

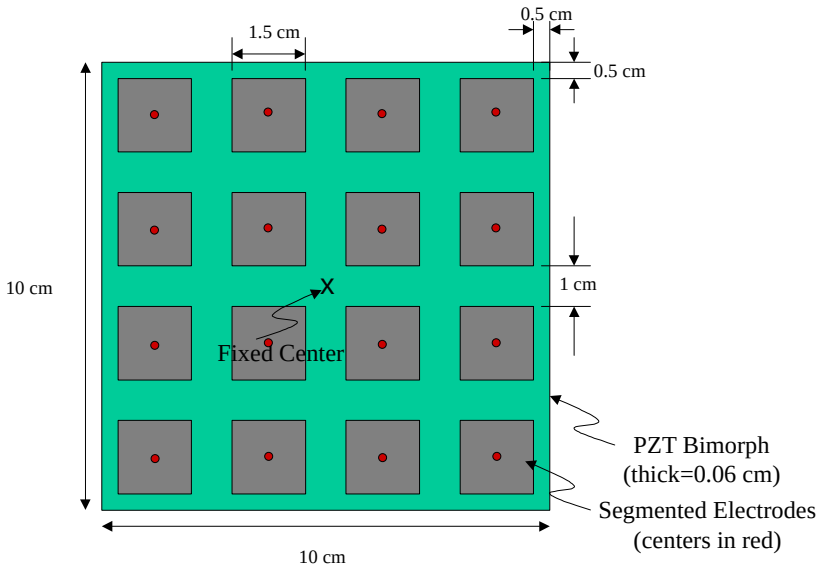

Figure 6-4. Bimorph PZT-5A plate with 4x4 electrode grid for discrete one-sided excitation demonstration.

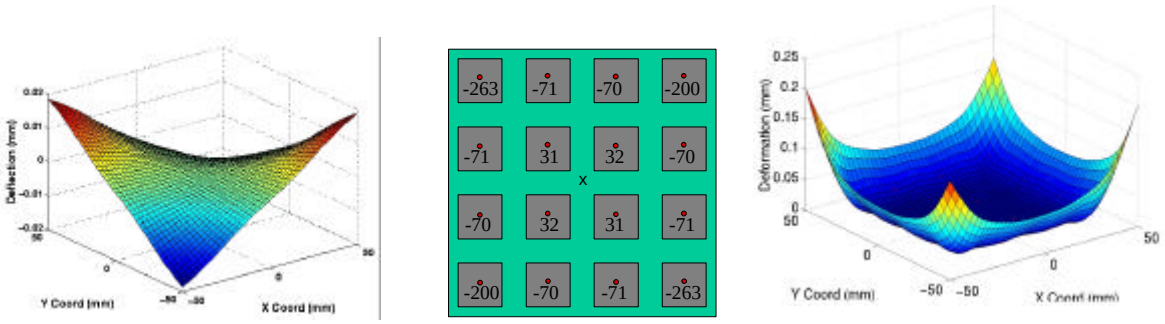

a. deformed shape b. corrective excitation c. corrected profile

Figure 6-5. One-sided excitation example of PZT-5A bimorph wafer subjected to an arbitrary disturbance and corrected by using a 4x4 grid of electrodes**.**

electrode midpoints lie on the desired surface to less than 0.01% error. Note, however, that the wafer behavior between the electrode midpoints can be non-ideal, and large deviations from the desired surface are evident particularly at the edges. However, using a higher density electrode pattern can reduce this effect, and the relationship between charge resolution and optical quality is the subject of continuing research.

6.4 Control Algorithm Summary

Controlling the deformations of a thin-skin piezoelectric polymer material to optical tolerances using an electron gun presents many challenging problems. The first phase of this research has focused on the development of open-loop quasi-static shape control algorithms suitable for beams and plates. As the material response behavior is better characterized, these algorithms will be extended to relate the excitation voltages presented in this section to actual electron gun control parameters. A gradual progression away from the model-based controller toward a more robust closed-loop control will follow. The end goal of the control algorithm development is to yield an intelligent control system able to sense the mirror shape or resulting image quality and autonomously make incremental improvements to yield optimal performance.

This page intentionally left blank.

7. CONCLUSIONS

The goal of this LDRD program was to assess and advance the state of the art in the critical technologies needed to realize a fully deployable electron gun controlled piezoelectric thin-skin mirror. Toward this end, the project has helped to mature many of the critical enabling technologies. Deployable electron gun controlled thin-skin mirrors may enable performance never before achieved with space-based optical systems. As opposed to conventional shape control approaches whereby a comparatively rigid mirror structure is deformed at a few locations using discrete actuators, the deployability and shape control are integrated into the mirror material by making it out of a "smart material" such as a piezoelectric bimorph. The electron gun provides for a noncontact high resolution approach to remotely changing the shape of the deployed mirror, mitigating the need for myriads of individual discrete actuators required to attain high resolution surfaces from flexible films. Furthermore, the electron gun is ideally suited for space and the power requirements to operate the gun are achievable from a space platform. Consequently, this approach shows great promise for meeting NASA's long term areal density goals of < 1 Kg/m^2.

In this two year project, significant progress has been made in the critical areas of experimental test bed development, optical sensing, electron gun excitation, and shape control algorithms. A unique testbed featuring an 18 inch diameter vacuum chamber was developed to enable examination of the complex interaction of the electron gun and the piezoelectric material. Both coarse and fine surface measurement techniques have been implemented to aid material characterization and initial feedback control experiments. Application of these techniques proved the capability of the electron gun to make both fine (~100 nm) and coarse (~1mm) surface profile corrections. Realizing the needed dynamic range in a single system will require further progress in the area of multi-wavelength heterodyne interferometry. This technique was briefly examined in this program, but shows great promise as a full field measurement technique with adjustable resolution.

Secondary electron yield behavior was explored through manipulation of the electrode potential and the hysteretic material behavior was quantified. In addition, a single input single output closed-loop control experiment was conducted using electron gun excitation and a tip displacement measurement. This experimental facility will be the focus of continuing research progressing toward distributed shape control of thin-skin mirrors. Open-loop shape correction algorithms were developed using computer simulation. Using experimentally derived models, these algorithms solve the direct inverse problem to determine distributed excitations needed to correct surface profile errors. Verification experiments will be conducted in FY01 with the goal of developing a model-independent autonomous closed-loop controller.

This work has captured the interest of the remote sensing community. Results show that although this field of research is in its infancy, many of the technological barriers to realization of a deployable mirror are surmountable. The potential for dramatically improving the resolution and sensitivity of future space based optical systems warrants continued research in this field. Remaining technical issues to be considered include mirror

packaging and deployment, space environment effects on candidate mirror materials, high fidelity shape sensing methods, and robust distributed curvature compensation algorithms. These critical technical issues will continue to be studied in order to bring this technology to maturity.

REFERENCES

Crawley, E., de Luis, J., 1986, "Piezoelectric Actuators as Elements of Intelligent Structures," AIAA 27th Structural Dynamics and Materials Conference, San Antonio, TX, Conference Proceedings, pg. 1373.

Floro, J.A., Chason, E., and Lee, S.R., 1995, "Real Time Measurement of Epilayer Strain Using a Simplified Wafer Curvature Technique," SAND95-1731C, Sandia National Laboratories, Albuquerque, NM.

Forbes, F., Roddier, F., Poczulp, G., Pinches, C., Sweeny, G., and Dueck, R., 1989, "Segmented Bimorph Deformable Mirror," Journal of Physics E: Scientific Instruments, Vol. 22, pp. 402-405.

Goldstein, J., Yakowitz, H., 1977, "Electron Beam – Specimen Interaction," *Practical Scanning Electron Microscopy*, Plenum Press, New York.

Greschik, G., 1996, "Deployment of Dishes with Surface Discontinuities," *Journal of Spacecraft and Rockets*, Vol. 33, No. 4, pp. 569-574.

Hagood, N., Bent, A., Rodgers, J., 1995, "Anisotropic Actuation with Piezoelectric Fiber Composites," *Journal of Intelligent Material Systems and Structures*, Volume 6, May, pg. 338.

Hardy, J.W., Lefebyre, J.E., and Koliopoulos, 1997, "Real-Time Atmospheric Compensation," *Journal of the Optical Society of America*, Vol. 67, No. 3, pp. 360-369.

Hibbitt, Karlsson, & Sorensen, Inc, 1998, *Abaqus Standard/User's Manual*, version 5.8.

Hubbard, J., "Active Mirror Assembly", United States Patent #5,159,498 October 22, 1992

Kimball Physics Inc., 1997©, "*EMG-14 EGPS-14 Instruction Manual*," Wilton, New Hampshire.

Koshida, N., and Yoshida, S., 1983, "Secondary Electron Emissions from Polyvinylidene Fluoride (PVDF) Film," *Journal of Applied Physics*, Volume 22, Number 11, pg. 1744.

Main, J. A., Nelson, G. C., and Martin, J. W., 1998, "Electron Gun Control of Piezoelectric Materials," Conference Proceedings, SPIE Symposium on Smart Structures and Materials.

Main, J. A., Garcia, E., and Howard, D.,1993, "Optimal Placement and Sizing of Paired Piezoactuators in Beams and plates," *Smart Material and Structures*, Volume 3, pg. 373-381.

Marker, D.K., Carreras, R.A., Wilkes, J.M., Jenkins, C.H., Duneman, D.C., Rotge, J. R., and Hogge, C.B., 1998, "Optical Evaluation of Membrane Mirrors with Curvature," Proceedings of SPIE, Vol. 3430, p. 202-208.

Martin, J. W., Masters Thesis, “Control of Thin Film Membrane Mirrors,” University of Kentucky, Lexington, KY, December 1998.

Martin, J.W., Main, J.A., and Nelson, G.C., 1998, “Shape Control of Deployable Membrane Mirrors,” Proceedings of the ASME International Mechanical Engineering Congress and Exposition, Anaheim, CA, November 15-20, 1998.

MathWorks, "Matlab- The Language of Technical Computing," Version 5, Natick, MA 1999.

McMackin, L., Voelz, D. G., Fetrow, M. P., McIntire, H., Bishop, K. P., Kellum, M. J., 1998, “Multi-Wavelength Heterodyne Array System for Large Space Optics Control,” SPIE Proceedings European Symposium on Remote Sensing, Barcelona, Spain.

McMackin, L., Voelz, D.G., and Fetrow, M.P., 1997, “Multiple Wavelength Heterodyne Array Interferometry,” *Optics Express*, Vol. 1, No. 11, pp. 332-337.

Merkle, F., 1992, “Principles of Adaptive Optics”, SPIE Vol. 1782, pp. 95-104.

Moore, C., 1999, “The Gossamer Spacecraft Initiative”, in Proceedings of the Ultra-Lightweight Space Optics Conference, March 24-25, Napa, CA.

Morgan Matroc, Inc, 1993, “Guide to Modern Piezoelectric Ceramics”.

NASA, 1994,“The Natural Space Environment: Effects on Spacecraft,” Publication 5-341-2, March.

Rapp, Donald, 1996, *Prospects and Limitations of Technical Approaches for Ultra Lightweight Space Telescopes*, JPL Report D-13975, Sept. 30, 1996.

Redmond, J. M., Barney, P. S., Henson, T. D., Main, J. A., Martin, J. W., 1999, “Distributed Sensing and Shape Control of Piezoelectric Bimorph Mirrors”, Proceedings of the ASME International Mechanical Engineering Congress and Exposition, Nashville, TN, November 1999.

Robinson, K., 1998, “Optical Sensor Monitors Film Growth,” *Photonics Technology World*, September 1998, pp. 51-52.

Rogers, C.A, W.L. Stutzman, T.G. Campbell, J.M. Hedgepeth, 1993, “Technology Assessment and Development of Large Deployable Antennas,” *Journal of Aerospace Engineering*, Vol. 6, No. 1, pp. 34-54.

Sato, T., Ishida, H., and Ikeda, O., 1980, “Adaptive PVDF Piezoelectric Deformable Mirror System,” *Applied Optics*, Vol. 19, No. 9, pp. 1430-1434.

Steinhaus, E., and Lipson, S.G., 1979, “Bimorph Piezoelectric Flexible Mirror,” *Journal of the Optical Society of America*, Vol. 69, No. 3, pp. 478-481.

Susini, J., Labergerie, D., and Zhang, L., 1995, "Compact active/adaptive x-ray mirror: Bimorph piezoelectric flexible mirror", *Rev. Sci. Instrum*. Vol. 66 (2), pp. 2229-2231.

Tzou, H. S., 1989, "Development of a Light-Weight Robot End-Effector Using Polymeric Piezoelectric Bimorph," Proceedings IEEE International Conference on Robotics and Automation, pg. 1704-1709.

Voelz, D.G., McMakin, L., Boger, J.K., and Fetrow, M.P., 1997, "Double Exposure Heterodyne Imaging for Observing Line-of-Sight Deformation," *Optics Letters*, Vol. 22, No. 13, pp. 1027-1029.

Wang, B. T., Rogers, C., 1991, "Laminate Plate Theory for Spatially Distributed Induced Strain Actuators," *Journal of Composite Materials*, Volume 25, April, pg. 433.

Whetten, N. R., 1981, "Secondary Electron Emission," *CRC Handbook of Chemistry and Physics*, 62nd Edition, CRC Press, Inc., pp. E373-E374.

This page intentionally left blank.

DISTRIBUTION:

5 University of Kentucky
Department of Mechanical Engineering
Attention: Dr. John Main
521 CRMS Building
Lexington, KY 40506

3 Air Force Research Laboratory/VSSV
Attention: Dr. Steven Huybrechts (1)
Dr. Richard Erwin (1)
Dr. Arup Maji (1)
3550 Aberdeen Ave. SE
Kirtland AFB, NM 87117-5776

3 Air Force Research Laboratory/DEBS
Attention: Dr. David Voelz (1)
Dr. Dan Marker (1)
Dr. Richard Carrares (1)
3550 Aberdeen Ave. SE
Kirtland AFB, NM 87117

1 Air Force Research Laboratory/VSC
Attention: Alok Das
3550 Aberdeen Ave. SE
Kirtland AFB, NM 87117

2 NASA Langley Research Center
Attention: Garnett Horner, Ph.D. (1)
Richard Pappa (1)
4 West Taylor Street
Hampton, VA 23681

1 NASA LaRC
Attention: Christopher Moore
M/S 367
8 Langley Blvd.
Hampton, VA 23681

1 DARPA/DSO
Attention: Dr. Ephram Garcia
3701 North Fairfax Drive
Arlington, VA 22203-1714

2 Jet Propulsion Laboratory
Attention: Michael Lou
M/S 125-224 (1)
Artur Chmielewski
M/S 180-603 (1)
4800 Oak Grove Drive
Pasadena, CA 91109

3 NASA Marshal Space Flight Center
Attention: James Bilbro
DA01 Bldg. 4200 (1)
Mike Tinker
ED21 (1)
Whit Brantley (1)
MSFC, AL 35812

1 SRS Technologies
Attention: Jim Moore
500 Discovery Drive
Huntsville, AL 35758

1 United Applied Technologies
Attention: Rodney Bradford
11506 Gilleland Road.
P.O. Box 4303
Huntsville, AL 35815

1 Naval Research Laboratory
Attention: Mike Brown
Code 8220
Washington, DC 20375

1	MS 0321	Bill Camp, 9200
1	0501	Pat Barney, 2338
1	0501	Ming Lau, 2338
1	0501	Tony Smith, 2338
1	0555	Mark Garrett, 9122
1	0555	Bruce Hansche, 9122
1	0555	Rod May, 9126
1	0557	Tom Baca, 9125
1	0557	Chris O'Gorman, 9125
1	0557	Todd Simmermacher, 9124
1	0557	John Zepper, 9131

1	0825	Walt Rutledge, 9115
1	0826	Wahid Hermina, 9113
1	0828	Jaime Moya, 9132
1	0828	Marty Pilch, 9133
1	0834	Justine Johannes, 9114
1	0834	Art Ratzel, 9112
1	0835	Steve Kempka, 9111
1	0836	Richard Griffith, 9117
1	0836	Eugene Hertel, 9116
1	0837	James Peery, 9121
1	0841	Tom Bickel, 9100
1	0847	Jeff Dohner, 9124
1	0847	Rich Field, 9124
1	0847	Rob Leland, 9226
1	0847	David Martinez, 9124
1	0847	Hal Morgan, 9123
5	0847	Jim Redmond, 9124
1	0847	Dan Segalman, 9124
1	0847	Steve Wojtkiewicz, 9124
1	0965	Kurt Lanes, 5711
1	0970	Alvin Lang, 5730
1	0972	Andy Boye, 5710
1	0972	Stephen Gentry, 5722
1	0972	Jeffrey Kern, 5710
1	0972	Anthony Medina, 5720
1	0980	Philip Green, 5712
1	0980	Carter Grotbeck, 5712
5	0980	Tammy Henson, 5712
1	0980	Karen Jefferson, 5712
5	0980	Jeffrey Martin, 5712
1	0980	Gary Phipps, 5712
5	0980	Joe Wehlburg, 5712
1	1415	John Hunter, 1114
1	0188	LDRD Office, 01030
1	9018	Central Technical Files, 8945-1
2	0899	Technical Library, 9619
1	0612	Review & Approval Desk, 9612 for DOE/OSTI